Universiteit
Leiden
The Netherlands

Squaramide-based interpenetrated networks for load-bearing applications

Chen, Y.

Citation
Chen, Y. (2024, November 8). *Squaramide-based interpenetrated networks for load-bearing applications*. Retrieved from https://hdl.handle.net/1887/4108020

Version:	Publisher's Version
License:	Licence agreement concerning inclusion of doctoral thesis in the Institutional Repository of the University of Leiden
Downloaded from:	https://hdl.handle.net/1887/4108020

Note: To cite this publication please use the final published version (if applicable).

Chapter 3

Dithiolane-ene Photopolymerization of Covalent and Supramolecular Networks Permits Cyclic Compressive Loading in 3D Cell Culture

Filamentous supramolecular polymers provide a modular synthetic platform that emulates the biopolymers of the extracellular matrix in their structure and function. However, the materials are mechanically weak and challenged to mimic the properties of tissues that undergo cyclic compressive loading like cartilage. Herein, we explore the use of light-mediated chain growth polymerization of dithiolane and dithiolane-ene to simultaneously crosslink a network of nanoscale supramolecular filaments with covalent polymer macromonomers, yielding hybrid double network hydrogels that can sustain dynamic compression in 3D cell culture. Benefitting from the energy dissipation mechanisms accessible to supramolecular materials, they show cartilage-like mechanical characteristics, such as biomimetic stress responses to compression and relaxation that can be tuned according to component ratios and concentrations using light. 3D culture of human primary articular chondrocytes in the photocrosslinked hydrogels displayed increased deposition of sulfated-glycosaminoglycans. Exploiting the photoreactive macromonomers, we mechanically pattern the materials at cell relevant length scales and apply cyclic compressive loads up to 14 days. The enclosed covalent network fortification strategy combined with bioorthogonal light-mediated crosslinking provides a base to tune the mechanics of filamentous supramolecular biomaterials in both space and time for 3D cell culture to mimic tissues under compressive loads in development and disease.

This chapter was prepared as a research article: Ying Chen,[+] Dr. Ciqing Tong,[+] Merel L. Janssen, Isabel Sariol, Joeri A. J. Wondergem, Marijn van den Brink, Prof. Dr. Rob G. H. H. Nelissen, Prof. Dr. Doris Heinrich, Dr. Yolande F. M. Ramos* and Dr. Roxanne E. Kieltyka*

[+] These authors contributed equally to this work.

3.1 Introduction

Synthetic hydrogels that mimic features of the natural extracellular matrix (ECM) are essential to promote *in vivo* cell behaviors for applications in tissue engineering and regenerative medicine. In the ECM, matrix proteins (e.g., collagens, proteoglycans) create an environment where numerous biochemical, architectural, and mechanical cues change in both space and time.[1–3] While hydrogel stiffness is a widely recognized mechanical cue that has been examined extensively in shear, others that are strain- and time-dependent (e.g., strain-stiffening or viscoelasticity) are being increasingly shown to influence cell behaviors in complex developmental and disease processes.[4–7] Moreover, cell cultures within these hydrogels are studied in absence of external mechanical loads, yet numerous tissues (e.g., cardiovascular, musculoskeletal, cartilage) are subjected to them (e.g., compression, tension).[8] As an example, the mechanical loading of cartilage starts before birth, influencing chondrocyte proliferation, maturation, and synthesis of ECM proteins, ultimately providing a stiff and tough tissue that maintains the joint biomechanical properties throughout life.[9,10] Hence, synthetic polymer hydrogels that can sustain a range of mechanical loads and respond in a biomimetic manner are urgently needed to not only unravel cell behaviour in health and disease (e.g., osteoarthritis (OA)),[11] but also for the development of more effective cellular therapies.

The exceptional mechanical properties of cartilage tissue, namely its capacity to bear a wide range of compressive loads up to 18 MPa[12] with a low coefficient of friction is enabled by its extensive ECM proteins[13,14] synthesized by chondrocytes. Cartilage ECM is presented differentially across the tissue being subdivided into three zones, from the superficial and middle to the deep zone, and exhibiting distinct structure and mechanics.[13,15] A critical player is the pericellular matrix (PCM) that is immediately adjacent to the chondrocyte cell membrane, consisting of fibrillar and network type collagens (i.e., collagens II/VI/IX), fibronectin and proteoglycans (e.g., aggrecan), transducing both mechanical and biochemical signals from the tissue to the cell.[16] Together with the chondrocyte they form the chondron, that has distinct mechanical properties from the surrounding cartilage ECM with a Young's modulus of 40 kPa – 70 kPa versus 1 MPa, respectively.[11] The PCM changes in its presentation around the chondrocyte during development, in diseases such as OA, and synthetic hydrogel materials based on their mechanics can alter its presentation only a few hours after seeding.[11,17,18] As cartilage mechanics and architecture vary across the tissue, hydrogel materials that span this range in their properties can enrich the growing knowledge of chondrocyte biology providing opportunities to direct their behavior for tissue engineering applications.

Supramolecular polymers bear analogy to ECM proteins, such as collagens, based on their filamentous nanostructures and functions that emerge from the non-covalent assembly of small molecules.[19–24] Above a critical monomer concentration gel phase materials with complex mechanics (e.g., viscoelasticity, strain stiffening, plasticity) can be prepared and drive cell responses when decorated with the appropriate chemical and bioactive cues.[25,26] Despite the modular and flexible approach to their preparation, the resulting materials show low storage moduli (10 Pa – 100 Pa) due to the entanglement of the filaments.[27,28] Consequently, such supramolecular networks alone cannot be applied for *in vitro* culture applications where dynamic mechanical loads are used. One strategy in

synthetic hydrogels that can permit access to the mechanics of load bearing tissues, such as cartilage, involves the use of double networks.[29,30] Two polymers that are juxtaposed in their properties are combined, one that is brittle and the other ductile (e.g., acrylates, acrylamides), with chemical and/or physical crosslinks between them leading to stiff (E ~ 0.1- 1 MPa) and tough materials (toughness ~ 0.01 - 1 MJ/m^{-3}).[31,32] The brittle network dissipates the energy on deformation by fracturing easily whereas the ductile network provides support to yield high toughness. However, the exclusive use of covalent bonds in both networks limits recovery of the material because of their irreversible character. While the use of supramolecular filaments can overcome this challenge, their preparation protocols lack cytocompatibility (e.g., high temperature, solvents) hampering opportunities to study their biomimetic structure and mechanics on cell behaviour in 3D culture.[33–36]

In this study, we explore a bioorthogonal strategy involving ring opening photopolymerization of 1,2-dithiolane (DT) and norbornene (NB) to prepare double networks (**DN**) based on supramolecular filaments consisting of squaramide[37–39] monomers and covalent poly(ethylene glycol) polymers for their 3D cell culture under compressive mechanical loads. While the thiol-norbornene reaction is a widely used photo-click reaction to prepare hydrogels through a step-growth mechanism, we demonstrated that exchange of thiol for DT, that provides two thiyl radicals on UV exposure at 365 nm, can lead to polymer networks (**PN**) through a chain-growth mechanism based on thioether linkages from linear poly(ethylene glycol) macromonomers showing similar cell viabilities.[40] Moreover, this dithiolane-ene photopolymerization strategy was recently used to fabricate granular hydrogels.[41] We therefore became interested to apply this covalent network to supramolecular filaments (**SN**) to form and fortify the materials with UV exposure at the same wavelength through the simultaneous photopolymerization of DT and DT-NB. Because a chain-growth polymerization approach is taken, several covalent and supramolecular polymers can be involved in a crosslink permitting simultaneous formation of the covalent network and its crosslinking to the supramolecular filaments. We then leverage these hybrid supramolecular and covalent materials for the 3D cell culture of human primary articular chondrocytes under cyclic mechanical loads and read out nascent matrix deposition, gaining insight into the potential of this biomimetic materials class tune their behavior. Finally, we show that this photopolymerization strategy can be used to engineer spatially distinct mechanical domains, stiff and soft, within these supramolecular biomaterials opening the door to mimic developmental and disease conditions that evolve in space and time.

3.2 Results and Discussion

Design and preparation of the squaramide-based supramolecular and covalent polymer double network hydrogels

To prepare the DN hydrogels based on supramolecular and covalent polymers, we co-assembled tripodal squaramide-based supramolecular polymers with 10 mol% 1,2-dithiolane (DT) monomer (5

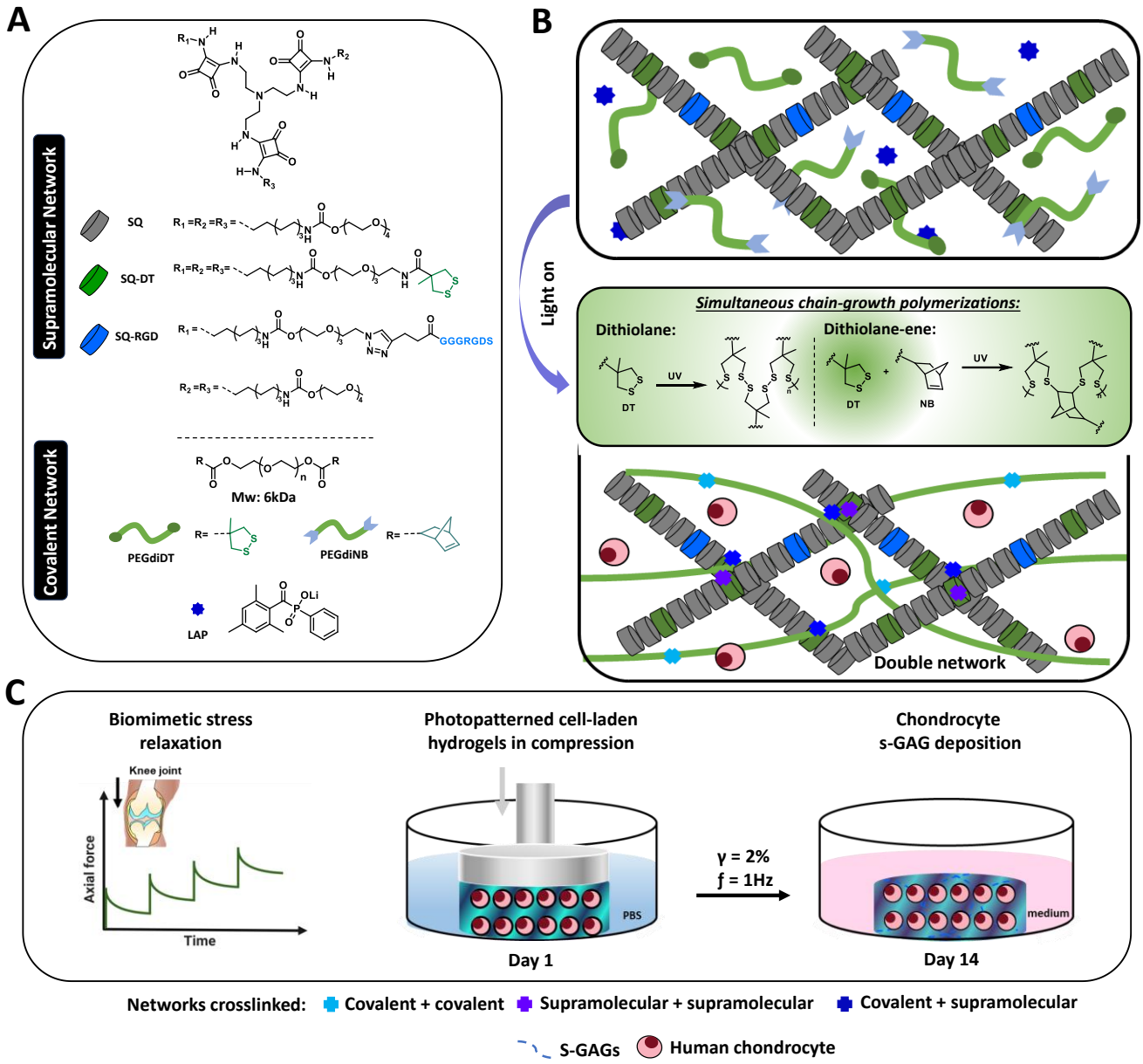

Scheme 1. (A) Supramolecular filament (**SN**: SQ, SQ-DT, and SQ-RGD) and covalent polymer (**PN**: PEGdiDT and PEGdiNB) components (*left*) to prepare **DN** hydrogels. (B) Mixing of components, DT and DT-NB photopolymerization to form **DN** hydrogels. (C) Biomimetic cartilage mechanical properties can be achieved in compression and release (*left*). The bioorthogonal photopolymerization approach in the **DN** hydrogel permits 3D human chondrocyte culture with cyclic compression leading to increased s-GAGs deposition (*middle and right, respectively*).

mM) (SN)[42] and linear 2-arm poly(ethylene glycol) (PEG) macromonomer (in total 3.6 wt%) end-functionalized with DT or NB (PN). More specifically, after sonication of a solution of the supramolecular filaments in phosphate buffered saline (pH 7.4) on ice, we added the DT and NB macromonomers and then brought them to room temperature (RT) to result in a hydrogel. Subsequently, photopolymerization of the soft hydrogel with UV light at 365-375 nm simultaneously formed a covalent network and crosslinked with the supramolecular filaments (SN) at the above component ratios. This result is supported by our earlier demonstrations that double addition of DT occurs across NB in the presence of LAP on covalent macromonomers[41] and poly(disulfide)s are formed on supramolecular polymers with UV exposure.[43] The hydrogels remained transparent (Figure S1) even after photopolymerization as observed in gel inversion tests; a feature that is needed for the eventual imaging of 3D cell cultures (Scheme 1).

Photocrosslinking of supramolecular and covalent polymer networks shows mechanical characteristics that outperform either component

We probed the effect of adding a second covalent network to the filamentous supramolecular network and DT-NB photopolymerization on hydrogel mechanical properties using oscillatory rheology. In time sweep measurements after 10 min UV exposure, we recorded **DN** storage moduli (G') greater than the individual components (Figure 1A). For the single network hydrogels, the **PN** (3.6 wt%) consisting of PEGdiDT (1.8 wt%) and PEGdiNB (1.8 wt%) with LAP (1.0 mM) showed a storage modulus of ~1 kPa, and the DT-crosslinked supramolecular polymer network **SN** reached ~3 kPa. For the double network material **DN**, mixing of the supramolecular **SN** and covalent **PN** networks resulted in a storage modulus of ~10 kPa (Figure 1A). The rise in the storage modulus is an order of magnitude greater than the sum of the **SN** and **PN**, and significantly greater than the pre-UV exposed hydrogel (~10 Pa), highlighting the synergy of mixing these two networks and their photocrosslinking. Additionally, the rate required to a reach a maximum in the storage modulus was reduced to 3 min for the **DN** as compared to the **SN** hydrogel that required ~10 min due to the absence of NB that rapidly undergoes photopolymerization with DT in the presence of **LAP** (Figure S2-S3). We then evaluated the change in hydrogel stiffness with short bursts of UV light in a sequential manner. The storage modulus increased in a stepwise manner rapidly with each step highlighting the rapid kinetics of the photopolymerization reaction, reaching equivalent values to the **DN** exposed for longer durations (e.g., 3 and 10 min). The response and duration of light used opens possibilities to modulate their mechanical properties in space and time as encountered in numerous complex biological process that occur in native tissues (Figure 1B).

We further examined different network compositions to deconvolute the origin of the dramatic increase in storage modulus on combining **SN** and **PN** (Figure S3). A semi-interpenetrating network **IPN** prepared at the same concentration as the **DN** without 10 mol% SQ-DT in the **SN** to crosslink both polymers gave a storage modulus of ~4 kPa. This result highlights the importance of the crosslinking of both **SN** and **PN** in the **DN** on the measured mechanical properties. On the other hand, incorporation of 10 mol% SQ-DT into the **SN** and exchange of the PEGdiDT for a PEG dithiol in the **PN** resulted in a storage modulus of ~3 kPa (Figure S4). As the DT unit is a bifurcated cross-linking unit that yields two

disulfides on ring opening with light leading to polymerization, its replacement with a thiol in the **PN** components abrogates opportunities for its formation and simultaneous crosslinking with the **SN**. To understand the contribution of the covalent network on the mechanical properties of the **DN**, we prepared a sample where only crosslinking of the **SN** would be possible by adding equivalent amounts of SQ-DT and PEG-NB without PEG-DT. Crosslinking of the supramolecular filaments alone did not yield the earlier recorded **DN** storage moduli (~2 kPa) (Figure S5). Overall, both the *in-situ* formation of the second **PN** and the crosslinking to the **SN** through the chain-growth photopolymerization of both networks is required to attain the stiffness of the **DN**.

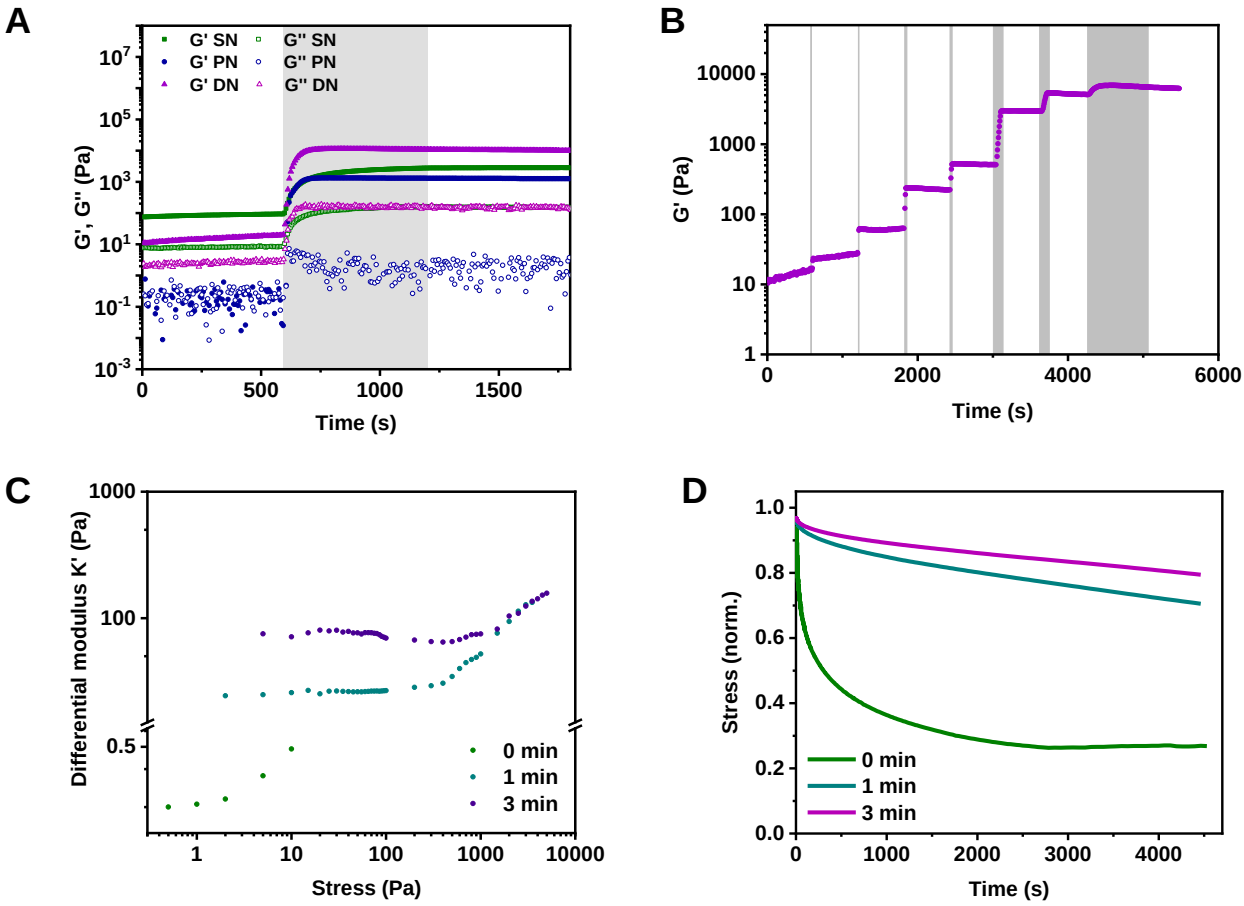

Figure 1. Oscillatory rheology data of hydrogels at RT: (A) Averaged (N=3 independent samples) time sweeps showing storage (G') and loss moduli (G") of **DN**, **PN** and **SN** with 10 min UV exposure. (B) Averaged (N=2 independent samples) time sweep showing storage modulus (G') with stepwise UV exposure of the **DN**. (C) Normalized stress relaxation behavior (σ/σ_0) (strain = 10%) of **DN** after different UV exposure times (0 min, 1 min, and 3 min). (D) Strain-stiffening behavior as indicated by differential modulus (K') of **DN** with different UV exposure times (0 min, 1 min and 3 min) measured using a pre-stress protocol. Light source parameters: ~10 mW/cm^2, λ = 320-500 nm, primary peak: 365 nm. Grey regions indicate UV exposure.

We then examined the range by which stiffness of the **DN** can be tuned by altering the reaction conditions. We modified the molar percentage of SQ-DT in **SN**, the total polymer concentration of the **DN**, and light source parameters while keeping the supramolecular polymer concentration constant (Table S1, Figure S6-S7). Increasing the concentration of the SQ-DT monomer from 0 to 10 mol% in the

supramolecular filament network resulted in an increase in storage modulus from ~4 kPa to ~10 kPa of the **DN** (Figure S6) pointing out that a small amount of co-assembled photoreactive monomer can significantly impact materials properties. Further increasing the covalent polymer concentration in the **DN** from 3.6 to 9.6 wt% resulted in an even greater increase in network stiffness raising the storage modulus up to ~21 kPa (Figure S7). Moreover, doubling the SQ concentration from 5 to 10 mM and reducing SQ-DT from 10 to 5 mol% resulted in similar storage moduli pointing out the salience of the covalent crosslinks and showcasing the modularity of the materials.

Since (dynamic) covalent bonds are made simultaneously between the **SN** and **PN** on photopolymerization, we evaluated their consequence on the **DN**s to self-recover after imposing a large strain (Figure S8-S9) in a cyclic manner through a step-strain test. After removal of a high strain (500%) from the **DN**, the initial storage modulus recovered ~51% as compared to the **SN** (8 mM) that reached 60% after two cycles. The extent of recovery of the **DN** increased to 64% when the **PN** increased to 7.2 wt%. This result confirms the formation of covalent bonds between both networks, but also highlights that the supramolecular interactions between filaments still contribute to the recovery of the materials at large strains on short timescales.

Covalent character is gained in the hydrogels complex mechanical characteristics

Native tissues show complex mechanical character in response to load that is time- and strain-dependent regulating cell processes such as long-distance communication, differentiation, and morphogenesis.[5–7,44,45] We therefore evaluated incorporation of the **PN** and its photopolymerization on the **DN** viscoelastic, viscoplastic and strain-stiffening properties in response to their shear deformation as supramolecular network filaments provide access to these properties. On subjecting the **DN** to 10% strain, the extent and rate of stress (σ) relaxation decreased with the UV exposure time. UV exposure for 1 min reduced the relaxed stress by ~44% after 75 minutes as compared to the non-UV exposed control. Increasing UV exposure to 3 min decreased relaxation by an additional ~10 % consistent with the increased covalent crosslinking through photopolymerization (Figure 1C). When compared against a **PN** (7.2 wt%) of equivalent storage modulus, the **DN** showed stress relaxation over the measuring period whereas the **PN** did not (Figure S10). This result demonstrates that the **SN** endows the **DN** with stress relaxation behavior through its entangled filament network.

Photopolymerization of both networks also resulted in changes to their susceptibility to plastic deformation in response to a constant shear stress in a creep and recovery test. UV exposure for 1 minute largely nullified the viscoplastic response of the **DN** to stress (300 Pa) as compared to the non-UV exposed control (Figure S11). We then examined the strain stiffening behavior of the **DN** using by a pre-stress method.[46] Non-linear responses were observed for all samples on comparison of the differential modulus (K') with increasing stress. The stress value at which the response of the sample deviates from linearity otherwise known as the critical stress, σ_c, increased significantly over several orders of magnitude for the supramolecular and covalent networks after UV exposure from 2.3 Pa (0 min) to 0.35 kPa (1 min) and 1 kPa (3 min) (Figure 1D, S12). Overall, the addition of the covalent polymer network and its chain-growth photopolymerization with the supramolecular filaments results in hydrogel mechanical properties that tend towards their covalent counterparts, but still retain features

that are inherently associated with those that are non-covalent and essential to mimic the mechanics of ECM proteins.

Highly compressive mechanical properties of DN hydrogels

Articular cartilage is a tissue that is subjected to cyclic compressive loading,[47] therefore understanding the mechanical behaviour of the covalent and supramolecular double network gels in compression is crucial. Axial force compression tests in the rheometer (Figure 2A) revealed significant differences in mechanical behaviour between the various networks from the collected compressive stress-strain profiles (Table S2). Compression of the **SN** hydrogel to ~2% of its initial height resulted in fracture at a stress of ~0.5 kPa (Figure 2B) demonstrating its brittle character and could not be characterized further. On the other hand, the **PN** endured up to ~40% strain (γ) prior to fracture with a stress increase of ~84 kPa consistent with formation of the covalent network and stable covalent crosslinks between the two networks. Addition of the **PN** to the **SN** forming the **DN**, boosted the compressive stress (~164 kPa) of the **DN** due to the supramolecular filaments albeit with a lower fracture strain (~20%) consistent with their mixing. For comparison, exchange of PEGdiDT for PEG dithiol or altering the ratio of NB in the **DN** (NB:DT ratio 1:1 or 1:2) only resulted in a slight improvement in compressive properties relative to **SN** (Figure S4 and S5) in line with earlier shear experiments. In the **IPN**, where the SQ-DT monomer that enables crosslinking of both networks is removed from the **SN**, a lower stress (~74 kPa) at fracture is recorded despite a similar fracture strain (~22%). Compression of the **DN** and **PN** hydrogels to 10% of their original height with a larger diameter geometry (20 mm), culminated in fracture of the **PN** (3.6 wt%) (Figure 2A) whereas the **DN** hydrogel maintained its form and removal of the compressive stress led to restoration of the initial shape. Importantly, the **DN** showed the most rapid increase in stress on compression of hydrogel with a greater compressive modulus (E) (~614 kPa) as compared to the **IPN** (~216 kPa) and **PN** (~62 kPa) (Figure 2C). The step-wise increase in compression modulus with the addition of the supramolecular filaments to the **PN** and their crosslinking through photopolymerization highlights the salient contribution of both features to the **DN** compressive properties. When compared to cartilage ECM, the compressive moduli obtained for these double networks is most like the PCM that envelops and aids to transduce mechanical signals from the surrounding ECM to the chondrocyte.

Compression relaxation cycles with increasing strains were performed to confirm the **SN**'s role as a sacrificial network and the influence of crosslinking on energy dissipation. With larger imposed strains, the hysteresis loops of the **DN** grew in area, indicating energy dissipated (E_D), from ~0.08 kJ/m^3 at 5% to ~3.93 kJ/m^3 at 20% strain (Figure 2D) validating the sacrificial contribution of the **SN**. In contrast, the **IPN** showed hysteresis loops with smaller areas (e.g., 1 kJ/m^3 at 20% strain) signaling that covalent crosslinks between the **SN** and **PN** are needed to enhance energy dissipation in the **DN**. In contrast, the **PN** showed a linear profile lacking hysteresis loops even at 40% strain (Figure 2D, S13-S14). As the toughening of the **DN** relies on the fracture of the **SN** as an energy dissipation mechanism, we compared the fracture energies of the various networks. The toughness of the **DN** (~13 kJ/m^3) was greater than the **SN** (4 J/m^3), pointing out the importance of the **PN** on its mechanical strength (Figure S15-S16). The **PN** (~10 kJ/m^3) showed decreased toughness relative to the **DN** due to the absence of the sacrificial

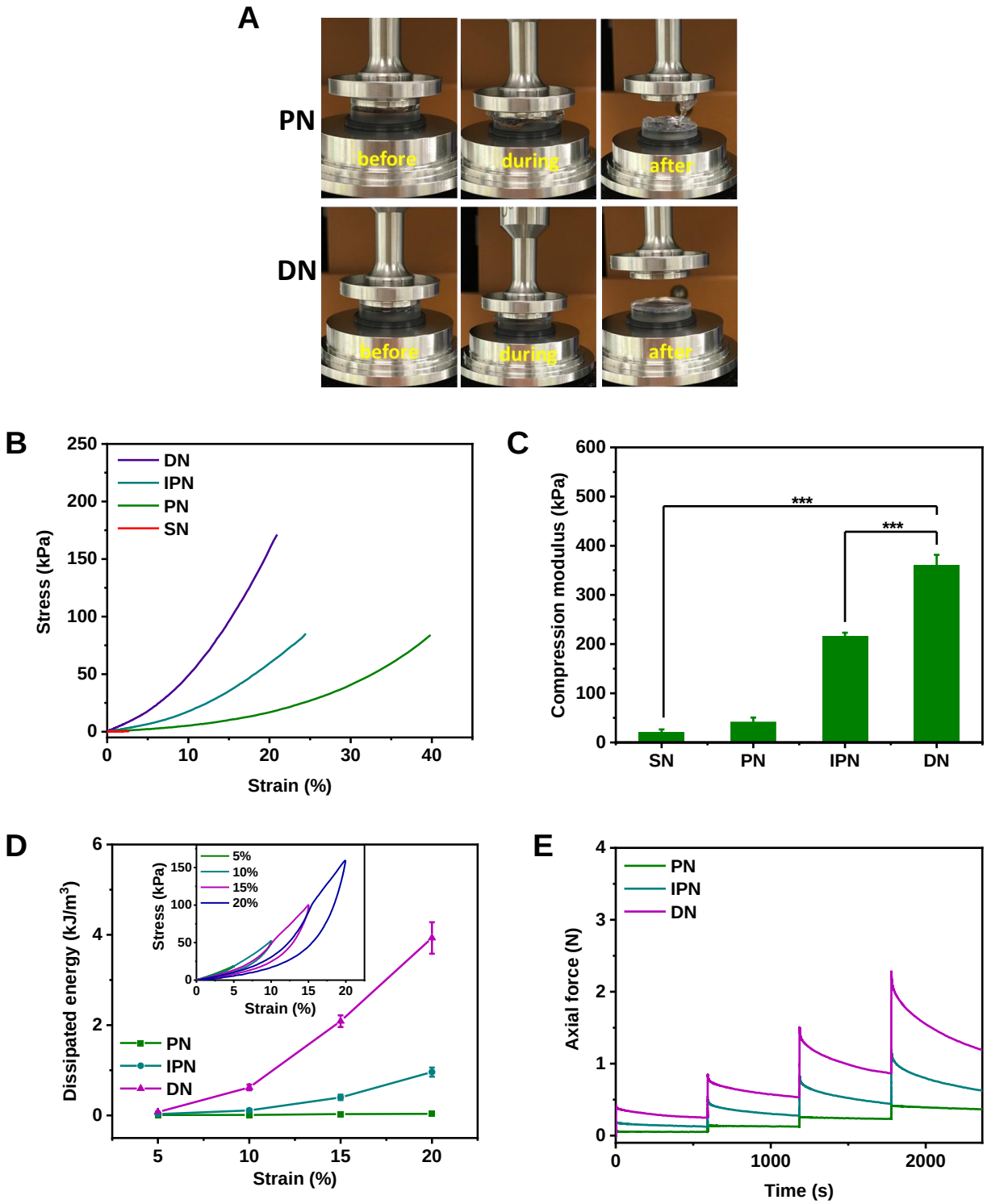

Figure 2. Compression behavior of the **SN**, **PN, IPN** and **DN** hydrogels: (A) Optical images displaying the photocrosslinked **PN** and **DN** before/during/after the compression experiments on the rheometer. (B) Uniaxial stress-strain (σ - γ) curves. (C) Measured compression moduli (E). *P*-values: ***<0.001, mean ± SD, N ≥ 3. (D) Measured dissipated energy (E_D) with increasing maximum strain (insert: uniaxial compression relaxation cycles of the **DN** at different maximum strains), Mean ± SD, N≥3. (E) Step-stress relaxation experiment with increasing strain (5%) at the start of each loading cycle.

network. However, its measured fracture energy was still greater than the **IPN** (~8 kJ/m^3) highlighting the contribution of the **PN** mechanical strength to the semi-interpenetrated network and the need for covalent crosslinking between both networks to reach the **DN** values (Figure S13-S14).

Rapid stress relaxation is a key feature of cartilage tissue that protects the joint from damage by dampening the mechanical load. Compressive loads were rapidly applied to the hydrogels and released monitoring their capacity to relax stress in a cyclic manner with increasing strain at the start of each loading cycle. The **DN** efficiently and promptly relaxed the stress in response to axial force (F) during each cycle (~36% – 48%) in a similar manner to cartilage,[48,49] whereas the **PN** hydrogel (Figure 2E) completely lacked this response profile. The **IPN** also relaxed the applied stress (44% - 46%) to a similar extent as the **DN** under identical conditions, but with a reduced axial force response to the applied load at the start of the cycle. This shows that the filamentous supramolecular polymers are important to guide this biomimetic stress relaxation behaviour within the **DN**, and crosslinking of both **SN** and **PN** through their photopolymerization provides a means to boost the axial force generated with cyclic compressive loading of the hydrogels.

Material characterizations of diverse DN hydrogels

To better understand the structural aspects of the gel that lead to the observed mechanical characteristics and influence their application for eventual 3D cell culture, we performed several imaging and equilibrium swelling assays. Cryo-TEM imaging of the **DN** before UV exposure confirmed that the supramolecular filaments remain present after the addition of poly(ethylene glycol) polymer. We observed flexible and micron-long entangled supramolecular filaments after incorporation of the **PN** (Figure S17). The retention of the **SN** after **PN** addition provides access to the biomimetic mechanical responses on compressive loading.

We further examined the hydrogels at the microscale after UV exposure by scanning electron microscopy (SEM). The pore size of the **DN** is smaller (~15 μm) than the **IPN** (~54 μm) that lacks crosslinking between the two networks through photopolymerization or that of the **PN** (~88 μm) (Figure S18). This finding supports the trends in the rheological data that show addition of a second network and its crosslinking result in increased storage and compressive moduli. We conducted an equilibrium swelling assay to determine the hydrogel stability and equilibrium water content (EWC) for their subsequent application in 3D cell culture. The **DN** showed consistent and minimal changes in swelling percentage after 3 minutes of UV exposure with maintenance in PBS or cell culture medium (DMEM) at 37 °C for more than 21 days, showing suitability for long-term cell culture experiments (Figure 3A). At the same time, the EWC values were measured for the various hydrogels after 3 minutes UV exposure (Figure 3B). While all hydrogels showed a EWC values above 95%, the **DN** showed a slightly lower EWC relative to the **SN** and **PN** that would be consistent with the increased network density and decreased pore sizes as measured in SEM. As the EWC value is well above 75% for the **DN**, transport of nutrients, and other biomolecules is expected[50] and through introduction of the second network and its crosslinking, stability for longer term culture periods can also be achieved.

To further quantify transport through the **PN** and **DN** after photopolymerization, we performed fluorescence recovery after photobleaching (FRAP) of fluorescently-labeled polymers through the

hydrogels. We compared diffusion of fluorescein isothiocyanate (FITC)-dextran (10 kDa and 70 kDa) against a small molecule fluoresceinamine (347 Da) for the various compositions at two different UV exposure times (0 and 3 min). All polymer sizes diffused at a sufficient rate in all the tested hydrogels in line with the length and time scales of nutrient diffusion and waste exchange involved in culturing encapsulated cells (Figure 3C). The diffusion coefficients (23.7, 6.5 and 2.0 $\mu m^2 s^{-1}$) of all FITC-dextran variants (347 Da, 10 kDa and 70 kDa) in the non-photopolymerized **DN** ((Figure S19A, Table S3) were comparable to the native squaramide-based hydrogels.[22] As the molecular weight of the polymers increased, their diffusion within the hydrogels and fluorescence recovery slowed down. After photopolymerization, the rate of diffusion in **DN** decreased (5.1, 3.5 and 0.7 $\mu m^2 s^{-1}$), but polymer exchange remained unblocked. For a **PN** (7.2 wt%) of similar stiffness to the **DN**, the diffusion of the fluorescent probes decreased further (1.6, 1.1 and 0.2 $\mu m^2 s^{-1}$) pointing at differences in architecture of the two materials (Figures S19B). The recovery half-times for all the measured hydrogels and fluorescent probes (Figure 3D) supported that diffusion slows down after photopolymerization but are within the same range as commonly used 3D culture substrates.[51]

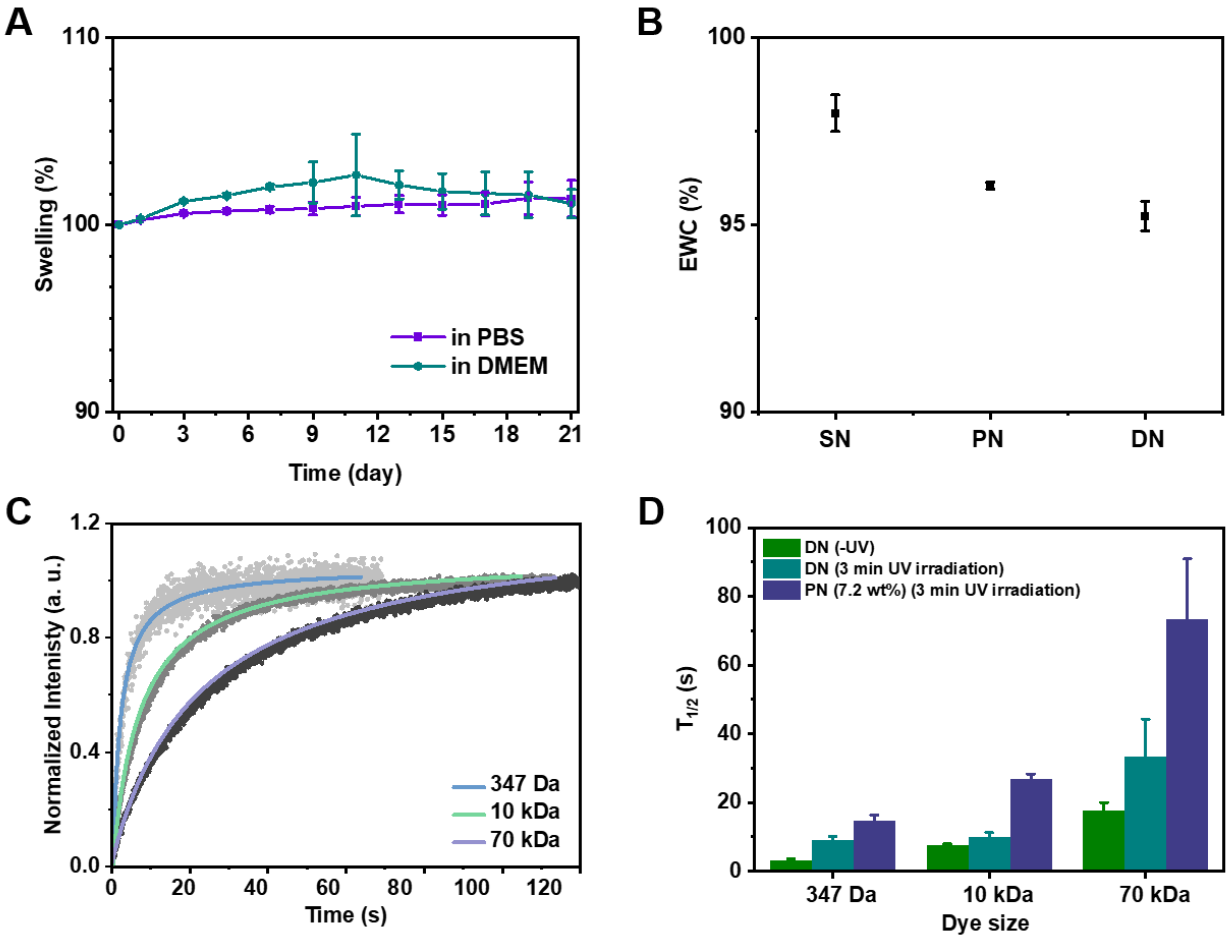

Figure 3. (A) Averaged (N = 3 independent samples) swelling percentage of **DN** hydrogel in PBS and cell culture medium DMEM containing 20% serum at 37 °C. (B) Averaged (N = 3) equilibrium water content (EWC) data for the different hydrogel networks. (C) FRAP characterization of **DN** hydrogel for three fluorescent probes of increasing molecular weight. Grey dots: Normalized intensity in the bleached spot; Lines: diffusion constant fit. (D) Extracted fluorescence recovery half-times of

different hydrogel compositions with and without 3 min UV irradiation using different sized fluorophores. Fluorophores: fluoresceinamine (347 Da); FITC-dextran (10 kDa); and FITC-dextran (70 kDa), mean ± SD, N≥3.

Mechanical loading effect the matrix growth in 3D culture

Cyclic compressive loading of the synthetic hydrogels *in vitro* provides unique opportunities to mimic the biomechanical environment that chondrocytes residing in cartilage are exposed to *in vivo*. Compressive loading of chondrocytes is known to prompt production of cartilaginous matrix proteins when in the physiological range, whereas excessive or hyperphysiological loading can lead to increased catabolic activity and decreased tissue production.[47,52] Therefore, we examined the potential to cyclically compress the chondrocyte-laden **DN** hydrogels using strains from 2-20% that mimic physiological to excessive loads in the joint.

Before performing cyclic loading experiments, we first evaluated the **DN** crosslinking chemistry on the 3D encapsulation of human primary articular chondrocytes (hPACs). We observed high viability (>80% / 5 d) of the hPACs after seeding and crosslinking of the **DN** using UV light (e.g., 0, 1 and 3 min) (Figure S20-S22). We then sought to understand hydrogel stiffness, inclusion of RGD and culture medium composition under free swelling (unloaded) conditions on hPACs viability and ECM production. We probed the effect of increased crosslinking and stiffness of the **DN** on their behaviour by varying the UV exposure times from 0 min (5 Pa) to 3 min (7.8 kPa) with SQ-RGD monomers co-assembled in the supramolecular filaments of the **DN** providing a handle for integrin targeting and chondrocyte mechanosensing of the hydrogels.[47] In the stiffer **DN** hydrogels, the chondrocytes appeared round whereas in softer hydrogels the cells were more spindle-like with less Alcian Blue staining reflecting a reduced sulphated-glycosaminoglycans (s-GAGs) deposition. When maintained in chondrogenic media with TGF-β1, all tested hydrogel conditions showed cartilaginous matrix surrounding the cells denoted by its intense Alcian Blue staining (Figure S23-S25). Hydrogels with greater stiffness (3 min UV, 7.8 kPa) displayed increased s-GAGs deposition as further quantified by the dimethylmethylene blue (DMMB) assay (Figure S26-S27). This finding is consistent with previous reports showing increased matrix deposition by chondrocytes in matrices of comparable stiffness.[53,54] Conversely, the culture of hPACs-laden **DN**s in chondrogenic expansion medium lacking TGF-β1 displayed minimal s-GAGs deposition, highlighting the relevance of both matrix stiffness and chondrogenic stimuli in triggering ECM deposition by hPACs (Figure S28). Subsequent removal of the RGD peptide showed limited effects on s-GAGs deposition suggesting that integrin engagement may not be necessary for matrix production under the tested culture conditions (Figure S27, S29). However, as earlier reports involving PEG-based covalent hydrogels showed that the presence of RGD ligands enhances matrix synthesis when mechanically stimulated,[55] we included them in the **DN** hydrogels to undergo dynamic mechanical loading with chondrocytes.

At this stage, we also exploited the photopolymerization chemistry to mechanically pattern the hydrogels with the aim of mimicking cartilage in development and disease. Alcian Blue staining of the photopatterned hydrogels revealed increased s-GAGs deposition by the hPACs in crosslinked areas (UV exposure 3 min) as compared to areas that were shielded from UV exposure by a striped photomask

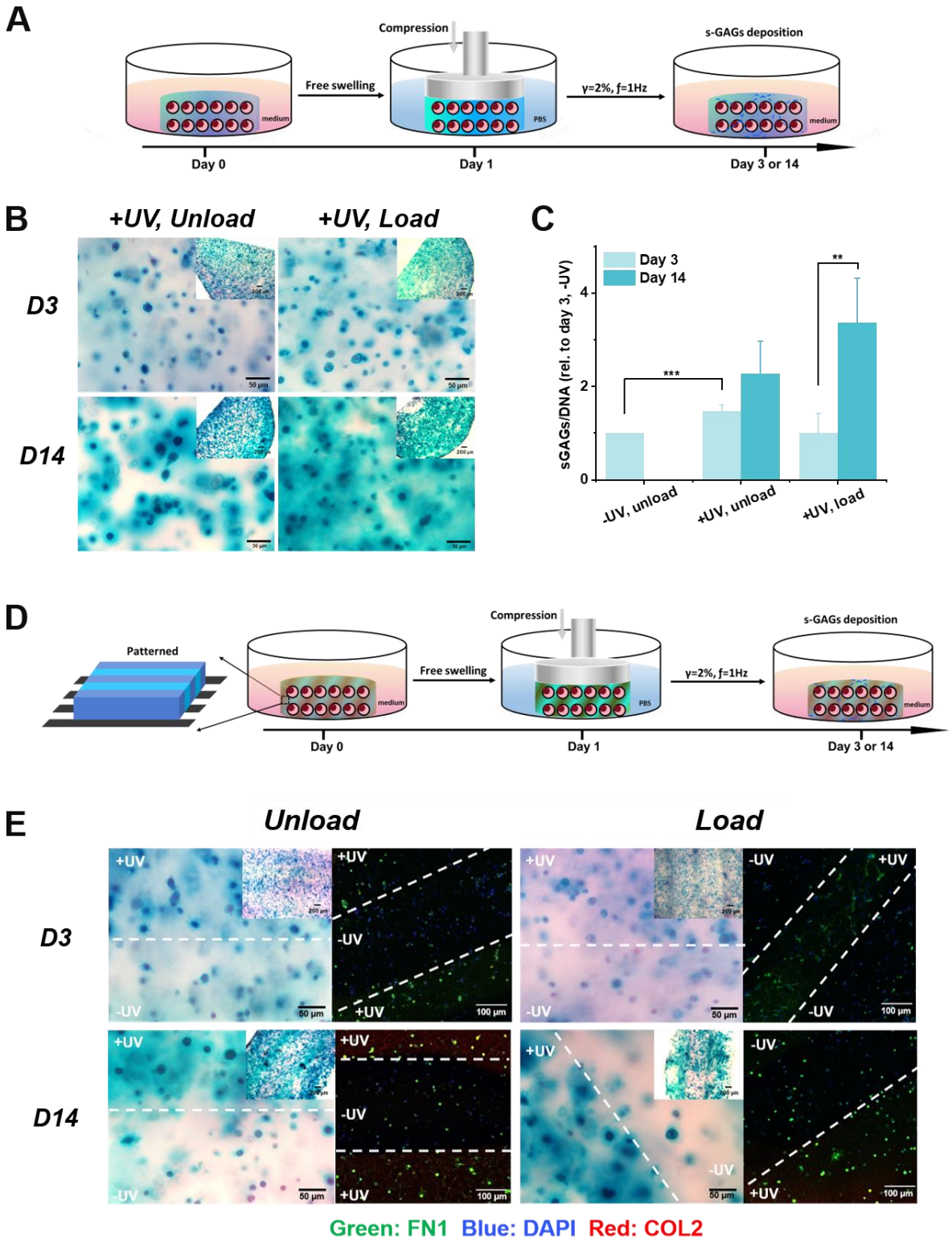

Figure 4. Cyclic compression of hPACs-laden **DN** hydrogels with SQ-RGD. (A) Scheme for dynamic mechanical loading during 3D chondrocyte culture. (B) Representative images for Alcian Blue and nuclear fast red staining after dynamic compression or in free swelling controls. (C) s-GAGs deposition, quantified by DMMB assay and normalized to DNA content, relative to day 3, -UV sample (5 donors total, 3-4 donors per condition). Mean + SEM; *P*-values Ttest: ** <0.01; *** <0.001. (D) Scheme for dynamic mechanical loading on 3D photopatterned hPACs-laden **DN** hydrogels. (E) Representative images for Alcian Blue

and nuclear fast red staining of s-GAGs deposition and overlay for immunofluorescence staining of fibronectin I and collagen II of photopatterned **DN**s after dynamic compression or in free swelling controls.

(Figure S24). To interrogate the capacity of the hPAC-laden **DN** hydrogels (UV exposure 3 min) to withstand physiological and excessive compressive loading, we performed dynamic mechanical compression experiments in a Mach-1 mechanical tester. Soft (2% strain, 1Hz) and heavy-loaded (20% strain, 5Hz) hPACs both displayed increased s-GAGs production compared to free swelling controls after 2 days (Figure S30) pointing out the ability of hydrogel matrices to transfer mechanical forces to the encapsulated cells. We observed little difference between soft and heavy loading regimes on s-GAGs deposition. However, as excessive loading using high strains is known to have detrimental effects on cartilage constructs over longer periods,[52] we selected a soft loading regime to investigate the effect of longer periods (e.g., 14 days) of dynamic compression on chondrocyte behaviour within the hydrogels.

DN hydrogels laden with hPACs were dynamically compressed for 14 days, with an intermediate sample being collected after 3 days of loading (Figure 4A). After 3 days, photocrosslinked samples (3 min UV) showed a consistent and significant increase in s-GAGs deposition when compared to non-crosslinked free swelling controls (Figure 4B-C) (0 min UV; 1.5-fold, P=7.3x10^{-5}). Loaded hydrogel constructs (3 min UV) compared to free swelling controls tend to deposit less s-GAGs at this time point (3 min UV; 0.6-fold, P=7.7x10^{-2}) (Figure 4B-C, S25, S31-S33, Table S4). After 14 days, photocrosslinked samples showed a general trend towards increased s-GAGs deposition compared to day 3 (3 min UV), with a larger increase for loaded (3.4-fold, P=6.3x10^{-3}) samples than for unloaded hydrogels (2.3-fold, P=6x10^{-2}), with some donor variation. Importantly, the s-GAGs deposited after the culture period extend beyond the cell surface, highlighting the contribution of the **SN** mechanics in accommodating deposited matrix despite the increased crosslink density[56] of the **DN** after UV exposure. Notably, photopatterned **DN** hydrogels possessing soft (0 min UV exposure) and stiff (UV exposure 3 min) regions in a single construct sustained dynamic mechanical loading, while the hydrogels without UV exposure were unstable. In line with the unloaded materials, higher levels of s-GAGs deposition can be observed in stiff regions against soft regions (Figure 4D). Pursuant to the previous findings, the differences became more evident after 14 days with more intense s-GAGs staining in the stiffer regions of the **DN**. Immunofluorescence staining of essential components of cartilaginous matrix fibronectin I (green) and collagen II (red) in photopatterned **DN**s showed higher fluorescence intensities in stiff regions in contrast to soft, especially for fibronectin I (Figure 4E), highlighting the contribution of matrix stiffness and culture duration on the production of cartilaginous matrix under dynamic mechanical compression. Taken together, these findings demonstrate the potential of the **DN** hydrogels to preserve chondrogenic characteristics of hPACs while stimulating the production and deposition of cartilaginous matrix under dynamic mechanical loading conditions.

3.3 Conclusion

We herein report a crosslinking strategy involving the photopolymerization of 1,2-dithioloane and norbornene to simultaneously crosslink and prepare supramolecular filament and covalent polymer networks in situ for 3D cell culture with cyclic compressive loading. The simultaneous chain-growth polymerizations of the DT and DT-NB groups provides access to the enhanced stiff and tough mechanical properties in compression not observed in either network on their own after photopolymerization. Strikingly, the use of filamentous supramolecular polymers in the **IPN** and **DN** yields hydrogels that display biomimetic cartilage-like mechanical responses to compression and release. The cytocompatible light-based crosslinking strategy and mechanical characteristics of the material permit cyclic compressive loading of 3D human primary articular chondrocytes for a two-week culture period that is challenging to achieve for single supramolecular networks as they as they unstable on their own and current double network preparation methods lack cytocompatibility for cell encapsulation. Within these hydrogels, the cells produce and deposit nascent matrix proteins that increase on compressive loading during the culture period providing insight into the consequence of **DN**s containing supramolecular filaments on chondrocyte behaviour. Further exploiting this photocrosslinking strategy, we demonstrate the patterning of soft and stiff domains in the hydrogels and their resultant loading in compression leads to contrasting cell responses. Importantly, this latent strategy involving 1,2-dithiolane and norbornene photopolymerization is a valuable addition to the commonly used polymerization chemistries to generate supramolecular and covalent double network hydrogels as it provides opportunities to spatiotemporally augment the mechanics of this biomimetic materials class to study and direct cell behaviour in 3D culture.

Reference

(1) Yamada, K. M.; Doyle, A. D.; Lu, J. Cell–3D Matrix Interactions: Recent Advances and Opportunities. *Trends in Cell Biology*. **2022**, 32 (10), 883.

(2) Qazi, T. H.; Blatchley, M. R.; Davidson, M. D.; Yavitt, F. M.; Cooke, M. E.; Anseth, K. S.; Burdick, J. A. Programming Hydrogels to Probe Spatiotemporal Cell Biology. *Cell Stem Cell* **2022**, *29* (5), 678.

(3) Huang, G.; Li, F.; Zhao, X.; Ma, Y.; Li, Y.; Lin, M.; Jin, G.; Lu, T. J.; Genin, G. M.; Xu, F. Functional and Biomimetic Materials for Engineering of the Three-Dimensional Cell Microenvironment. *Chem Rev* **2017**, *117* (20), 12764.

(4) Rizwan, M.; Ling, C.; Guo, C.; Liu, T.; Jiang, J.-X.; Bear, C. E.; Ogawa, S.; Shoichet, M. S. Viscoelastic Notch Signaling Hydrogel Induces Liver Bile Duct Organoid Growth and Morphogenesis. *Adv Healthc Mater* **2022**, *11* (23), 2200880.

(5) Chaudhuri, O.; Cooper-White, J.; Janmey, P. A.; Mooney, D. J.; Shenoy, V. B. Effects of Extracellular Matrix Viscoelasticity on Cellular Behaviour. *Nature* **2020**, *584* (7822), 535.

(6) Chaudhuri, O.; Gu, L.; Klumpers, D.; Darnell, M.; Bencherif, S. A.; Weaver, J. C.; Huebsch, N.; Lee, H.; Lippens, E.; Duda, G. N.; Mooney, D. J. Hydrogels with Tunable Stress Relaxation Regulate Stem Cell Fate and Activity. *Nat Mater* **2016**, *15* (3), 326.

(7) Storm, C.; Pastore, J. J.; MacKintosh, F. C.; Lubensky, T. C.; Janmey, P. A. Nonlinear Elasticity in Biological Gels. *Nature* **2005**, *435* (7039), 191.

(8) Guimarães, C. F.; Gasperini, L.; Marques, A. P.; Reis, R. L. The Stiffness of Living Tissues and Its Implications for Tissue Engineering. *Nat Rev Mater* **2020**, *5* (5), 351.

(9) Shea, C. A.; Rolfe, R. A.; Murphy, P. The Importance of Foetal Movement for Co-Ordinated Cartilage and Bone Development in Utero. *Bone Joint Res* **2015**, *4* (7), 105.

(10) Lee, H.-Y.; Han, L.; Roughley, P. J.; Grodzinsky, A. J.; Ortiz, C. Age-Related Nanostructural and Nanomechanical Changes of Individual Human Cartilage Aggrecan Monomers and Their Glycosaminoglycan Side Chains. *J Struct Biol* **2013**, *181* (3), 264.

(11) Guilak, F.; Nims, R. J.; Dicks, A.; Wu, C. L.; Meulenbelt, I. Osteoarthritis as a Disease of the Cartilage Pericellular Matrix. *Matrix Biology*. **2018**, *71*, 40.

(12) Hodge, W. A.; Fijan, R. S.; Carlson, K. L.; Burgess, R. G.; Harris, W. H.; Mann, R. W. Contact Pressures in the Human Hip Joint Measured in Vivo. *Proc Natl Acad Sci U S A* **1986**, *83* (9), 2879.

(13) Liu, M.; Zeng, X.; Ma, C.; Yi, H.; Ali, Z.; Mou, X.; Li, S.; Deng, Y.; He, N. Injectable Hydrogels for Cartilage and Bone Tissue Engineering. *Bone Res* **2017**, *5* (1), 17014.

(14) Fox, A. J. S.; Bedi, A.; Rodeo, S. A. The Basic Science of Articular Cartilage: Structure, Composition, and Function. *Sports Health* **2009**, *1* (6), 461.

(15) Antons, J.; Marascio, M. G. M.; Nohava, J.; Martin, R.; Applegate, L. A.; Bourban, P. E.; Pioletti, D. P. Zone-Dependent Mechanical Properties of Human Articular Cartilage Obtained by Indentation Measurements. *Journal of Materials Science: Materials in Medicine*. **2018**, *29* (5), 57.

(16) Wilusz, R. E.; Sanchez-Adams, J.; Guilak, F. The Structure and Function of the Pericellular Matrix of Articular Cartilage. *Matrix Biology*. **2014**, *39*, 25.

(17) Loebel, C.; Kwon, M. Y.; Wang, C.; Han, L.; Mauck, R. L.; Burdick, J. A. Metabolic Labeling to Probe the Spatiotemporal Accumulation of Matrix at the Chondrocyte–Hydrogel Interface. *Adv Funct Mater* **2020**, *30* (44), 1.

(18) Alexopoulos, L. G.; Williams, G. M.; Upton, M. L.; Setton, L. A.; Guilak, F. Osteoarthritic Changes in the Biphasic Mechanical Properties of the Chondrocyte Pericellular Matrix in Articular Cartilage. *J Biomech* **2005**, *38* (3), 509.

(19) Hafeez, S.; Decarli, M. C.; Aldana, A.; Ebrahimi, M.; Ruiter, F. A. A.; Duimel, H.; van Blitterswijk, C.; Pitet, L. M.; Moroni, L.; Baker, M. B. In Situ Covalent Reinforcement of a Benzene-1,3,5-Tricarboxamide Supramolecular Polymer Enables Biomimetic, Tough, and Fibrous Hydrogels and Bioinks. *Adv Mater* **2023**, *35* (35), 2301242.

(20) Kuang, Y.; Yao, Z.-F.; Lim, S.; Ngo, C.; Rocha, M. A.; Fishman, D. A.; Ardoña, H. A. M. Biomimetic Sequence-Templating Approach toward a Multiscale Modulation of Chromogenic Polymer Properties. *Macromolecules* **2023**, *56* (12), 4526.

(21) Zhu, Y.; Shmidov, Y.; Harris, E. A.; Theus, M. H.; Bitton, R.; Matson, J. B. Activating Hidden Signals by Mimicking Cryptic Sites in a Synthetic Extracellular Matrix. *Nat Commun* **2023**, *14* (1), 3635.

(22) Monti, M.; Scarel, E.; Hassanali, A.; Stener, M.; Marchesan, S. Diverging Conformations Guide Dipeptide Self-Assembly into Crystals or Hydrogels. *Chem Comm* **2023**, *59* (73), 10948.

(23) Sikder, A.; Sarkar, J.; Barman, R.; Ghosh, S. Directional Supramolecular Assembly of π-Amphiphiles with Tunable Surface Functionality and Impact on the Antimicrobial Activity. *J Phys Chem B* **2019**, *123* (33), 7169.

(24) Gruschwitz, F. V; Hausig, F.; Schüler, P.; Kimmig, J.; Hoeppener, S.; Pretzel, D.; Schubert, U. S.; Catrouillet, S.; Brendel, J. C. Shear-Thinning and Rapidly Recovering Hydrogels of Polymeric Nanofibers Formed by Supramolecular Self-Assembly. *Chemistry of Materials* **2022**, *34* (5), 2206.

(25) Liu, T.; van den Berk, L.; Wondergem, J. A. J.; Tong, C.; Kwakernaak, M. C.; Braak, B. ter; Heinrich, D.; van de Water, B.; Kieltyka, R. E. Squaramide-Based Supramolecular Materials Drive HepG2 Spheroid Differentiation. *Adv Healthc Mater* **2021**, *10* (11), e2001903.

(26) Diba, M.; Spaans, S.; Hendrikse, S. I. S.; Bastings, M. M. C.; Schotman, M. J. G.; van Sprang, J. F.; Wu, D. J.; Hoeben, F. J. M.; Janssen, H. M.; Dankers, P. Y. W. Engineering the Dynamics of Cell Adhesion Cues in Supramolecular Hydrogels for Facile Control over Cell Encapsulation and Behavior. *Adv Mater* **2021**, *33* (37), 2008111.

(27) Chivers, P. R. A.; Smith, D. K. Shaping and Structuring Supramolecular Gels. *Nat Rev Mater* **2019**, *4* (7), 463.

(28) Tong, C.; Liu, T.; Saez Talens, V.; Noteborn, W. E. M.; Sharp, T. H.; Hendrix, M. M. R. M.; Voets, I. K.; Mummery, C. L.; Orlova, V. V.; Kieltyka, R. E. Squaramide-Based Supramolecular Materials for Three-Dimensional Cell Culture of Human Induced Pluripotent Stem Cells and Their Derivatives. *Biomacromolecules* **2018**, *19* (4), 1091.

(29) Aldana, A. A.; Houben, S.; Moroni, L.; Baker, M. B.; Pitet, L. M. Trends in Double Networks as Bioprintable and Injectable Hydrogel Scaffolds for Tissue Regeneration. *ACS Biomater Sci Eng* **2021**, *7* (9), 4077.

(30) Means, A. K.; Grunlan, M. A. Modern Strategies To Achieve Tissue-Mimetic, Mechanically Robust Hydrogels. *ACS Macro Lett* **2019**, *8* (6), 705.

(31) Gong, J. P. Why Are Double Network Hydrogels so Tough? *Soft Matter* **2010**, *6* (12), 2583.

(32) Gong, J. P.; Katsuyama, Y.; Kurokawa, T.; Osada, Y. Double-Network Hydrogels with Extremely High Mechanical Strength. *Adv Mater* **2003**, *15* (14), 1155.

(33) Yasui, T.; Zheng, Y.; Nakajima, T.; Kamio, E.; Matsuyama, H.; Gong, J. P. Rate-Independent Self-Healing Double Network Hydrogels Using a Thixotropic Sacrificial Network. *Macromolecules* **2022**, *55* (21), 9547.

(34) Sun, W.; Xue, B.; Li, Y.; Qin, M.; Wu, J.; Lu, K.; Wu, J.; Cao, Y.; Jiang, Q.; Wang, W. Polymer-Supramolecular Polymer Double-Network Hydrogel. *Adv Funct Mater* **2016**, *26* (48), 9044.

(35) Wei, Q.; Chang, Y.; Ma, G.; Zhang, W.; Wang, Q.; Hu, Z. One-Pot Preparation of Double Network Hydrogels via Enzyme-Mediated Polymerization and Post-Self-Assembly for Wound Healing. *J Mater Chem B* **2019**, *7*, 6195.

(36) Liang, Y.; Wang, K.; Li, J.; Wang, H.; Xie, X. Q.; Cui, Y.; Zhang, Y.; Wang, M.; Liu, C. Sen. Low-Molecular-Weight Supramolecular-Polymer Double-Network Eutectogels for Self-Adhesive and Bidirectional Sensors. *Adv Funct Mater* **2021**, *31* (45), 2104963.

(37) Bujosa, S.; Doncel-Giménez, A.; Bäumer, N.; Fernández, G.; Ortí, E.; Costa, A.; Rotger, C.; Aragó, J.; Soberats, B. Thermoreversible Polymorph Transitions in Supramolecular Polymers of Hydrogen-Bonded Squaramides. *Angewandte Chemie International Edition* **2022**, *61* (47), e202213345.

(38) Ramos, J.; Arufe, S.; Martin, H.; Rooney, D.; Elmes, R. B. P.; Erxleben, A.; Moreira, R.; Velasco-Torrijos, T. Glycosyl Squaramides, a New Class of Supramolecular Gelators. *Soft Matter* **2020**, *16* (34), 7916.

(39) Saez Talens, V.; Davis, J.; Wu, C. H.; Wen, Z.; Lauria, F.; Gupta, K. B. S. S.; Rudge, R.; Boraghi, M.; Hagemeijer, A.; Trinh, T. T.; Englebienne, P.; Voets, I. K.; Wu, J. I.; Kieltyka, R. E. Thiosquaramide-Based Supramolecular Polymers: Aromaticity Gain in a Switched Mode of Self-Assembly. *J Am Chem Soc* **2020**, *142* (47), 19907.

(40) Tong, C.; Wondergem, J. A. J.; Heinrich, D.; Kieltyka, R. E. Photopatternable, Branched Polymer Hydrogels Based on Linear Macromonomers for 3D Cell Culture Applications. *ACS Macro Lett* **2020**, *9* (6), 882.

(41) Nelson, B. R.; Kirkpatrick, B. E.; Miksch, C. E.; Davidson, M. D.; Skillin, N. P.; Hach, G. K.; Khang, A.; Hummel, S. N.; Fairbanks, B. D.; Burdick, J. A.; Bowman, C. N.; Anseth, K. S. Photoinduced Dithiolane Crosslinking for Multiresponsive Dynamic Hydrogels. *Adv Mater* **2023**, 3, e2211209.

(42) Tong, C.; Wondergem, J. A. J.; van den Brink, M.; Kwakernaak, M. C.; Chen, Y.; Hendrix, M. M. R. M.; Voets, I. K.; Danen, E. H. J.; Le Dévédec, S.; Heinrich, D.; Kieltyka, R. E. Spatial and Temporal Modulation of Cell Instructive Cues in a Filamentous Supramolecular Biomaterial. *ACS Appl Mater Interfaces* **2022**, *14* (15), 17042.

(43) Tong, C.; Wondergem, J. A. J.; van den Brink, M.; Kwakernaak, M. C.; Chen, Y.; Hendrix, M. M. R. M.; Voets, I. K.; Danen, E. H. J.; Le Dévédec, S.; Heinrich, D.; Kieltyka, R. E. Spatial and Temporal Modulation of Cell Instructive Cues in a Filamentous Supramolecular Biomaterial. *ACS Appl Mater Interfaces* **2022**, *14* (15), 17042.

(44) Hall, M. S.; Alisafaei, F.; Feng, X.; Hui, C.-Y.; Shenoy, V. B.; Wu, M.; Weitz, D. A. Fibrous Nonlinear Elasticity Enables Positive Mechanical Feedback between Cells and ECMs. *Proceedings of the National Academy of Science* **2016**, *113* (49), 14043.

(45) Rudnicki, M. S.; Cirka, H. A.; Aghvami, M.; Sander, E. A.; Wen, Q.; Billiar, K. L. Nonlinear Strain Stiffening Is Not Sufficient to Explain How Far Cells Can Feel on Fibrous Protein Gels. *Biophys J* **2013**, *105* (1), 11.

(46) Broedersz, C. P.; Kasza, K. E.; Jawerth, L. M.; Münster, S.; Weitz, D. A.; MacKintosh, F. C. Measurement of Nonlinear Rheology of Cross-Linked Biopolymer Gels. *Soft Matter* **2010**, *6* (17), 4120.

(47) Sanchez-Adams, J.; Leddy, H. A.; McNulty, A. L.; O'Conor, C. J.; Guilak, F. The Mechanobiology of Articular Cartilage: Bearing the Burden of Osteoarthritis. *Curr Rheumatol Rep* **2014**, *16* (10), 451.

(48) Shao, X.; Goh, J. C. H.; Hutmacher, D. W.; Lee, E. H.; Zigang, G. Repair of Large Articular Osteochondral Defects Using Hybrid Scaffolds and Bone Marrow-Derived Mesenchymal Stem Cells in a Rabbit Model. *Tissue Eng* **2006**, *12* (6), 1539.

(49) Li, L. P.; Herzog, W.; Korhonen, R. K.; Jurvelin, J. S. The Role of Viscoelasticity of Collagen Fibers in Articular Cartilage: Axial Tension versus Compression. *Med Eng Phys* **2005**, *27* (1), 51.

(50) Harrass, K.; Krüger, R.; Möller, M.; Albrecht, K.; Groll, J. Mechanically Strong Hydrogels with Reversible Behaviour under Cyclic Compression with MPa Loading. *Soft Matter* **2013**, *9* (10), 2869.

(51) Urciuolo, A.; Giobbe, G. G.; Dong, Y.; Michielin, F.; Brandolino, L.; Magnussen, M.; Gagliano, O.; Selmin, G.; Scattolini, V.; Raffa, P.; Caccin, P.; Shibuya, S.; Scaglioni, D.; Wang, X.; Qu, J.; Nikolic, M.; Montagner, M.; Galea,

G. L.; Clevers, H.; Giomo, M.; De Coppi, P.; Elvassore, N. Hydrogel-in-Hydrogel Live Bioprinting for Guidance and Control of Organoids and Organotypic Cultures. *Nat Commun* **2023**, *14* (1), 3128.
(52) Houtman, E.; Tuerlings, M.; Riechelman, J.; Suchiman, E. H. E. D.; van der Wal, R. J. P.; Nelissen, R. G. H. H.; Mei, H.; Ramos, Y. F. M.; Coutinho de Almeida, R.; Meulenbelt, I. Elucidating Mechano-Pathology of Osteoarthritis: Transcriptome-Wide Differences in Mechanically Stressed Aged Human Cartilage Explants. *Arthritis Res Ther* **2021**, *23* (1), 215.
(53) Tan, Y.; Huang, H.; Ayers, D. C.; Song, J. Modulating Viscoelasticity, Stiffness, and Degradation of Synthetic Cellular Niches via Stoichiometric Tuning of Covalent versus Dynamic Noncovalent Cross-Linking. *ACS Cent Sci* **2018**, *4* (8), 971.
(54) Lee, H.; Gu, L.; Mooney, D. J.; Levenston, M. E.; Chaudhuri, O. Mechanical Confinement Regulates Cartilage Matrix Formation by Chondrocytes. *Nat Mater* **2017**, *16* (12), 1243.
(55) Villanueva, I.; Weigel, C. A.; Bryant, S. J. Cell–Matrix Interactions and Dynamic Mechanical Loading Influence Chondrocyte Gene Expression and Bioactivity in PEG-RGD Hydrogels. *Acta Biomater* **2009**, *5* (8), 2832.
(56) Loebel, C.; Kwon, M. Y.; Wang, C.; Han, L.; Mauck, R. L.; Burdick, J. A. Metabolic Labeling to Probe the Spatiotemporal Accumulation of Matrix at the Chondrocyte–Hydrogel Interface. *Adv Funct Mater* **2020**, *30* (44), 1909802.

Supporting information

3.1. Materials and methods

Materials

All chemicals and reagents for synthesis were obtained from Sigma Aldrich and directly used without further purification. Deuterated solvent for NMR experiments were obtained from Euriso-top. Water was deionized before use. Lacey carbon 200 mesh grids were purchased from Electron Microscopy Sciences. Dulbecco's phosphate buffered saline (DPBS, pH=7.4) was purchased from Sigma Aldrich. Dulbecco's modified Eagle medium (DMEM) was received from Gibco, Life Technologies. Fetal bovine serum (FBS) was procured from Biowest. The antibiotics penicillin and streptomycin were purchased from Gibco. Collagenase Type I was obtained from Worthington Biochemical Corporation. Calcein AM, Propidium Iodide (PI), Alcian Blue 8-GX, Nuclear fast red-aluminum sulfate, and normal goat serum were purchased from Sigma Aldrich. The goat anti-mouse Alexa Fluor 647 and goat anti-rabbit Alexa Fluor 488 were obtained from Abcam. µ-Slide 15 Well 3D chambered coverplates were purchased from Ibidi. Polydimethylsiloxane (PDMS) (Sylgard 184 Silicon Elastomer Kit, Dow Corning), silicon wafers and fluorosilane (1H,1H,2H,2H-perfluorooctyltrichlorosilane) from VWR chemicals, Siegert Wafers and Sigma-Aldrich, respectively. Monomers SQ, SQ-DT, SQ-RGD, PEGdiNB (6 kDa), and PEGdiDT (6 kDa) were synthesized as previously described.[1] All compounds were stored at -20°C prior to further use.

Methods

^{1}H-NMR and ^{13}C-NMR spectra were collected at room temperature (RT) on a Bruker DMX-400 (400 MHz). Oscillatory rheology experiments were performed at RT on a Discovery Hybrid Rheometer (DHR-2) from TA Instruments on a quartz lower plate (20 mm) and a aluminum upper plate (20 mm) using a fixed gap of 300 µm. UV light (λ = 320-500 nm, primary peak: 365 nm) was applied through an Omnicure S2000 high-pressure mercury light source from Excelitas connected to the rheometer through a UV light guide accessory (5 mm diameter). The UV intensity was calibrated using a Silverline radiometer sensor (20 mm) designed for the quartz parallel plate. Compression experiments were performed on this setup using aluminum upper plates with different diameters (8 mm and 20 mm) at a fixed gap of 1.2 mm and a maximum axial force of 50 N. Cryogenic electron microscope (cryo-EM) images were taken on a Talos L120C operating at 120 kV, samples were plunge frozen on a Vitrobot Mark IV, both from Thermo Fisher Scientific. Scanning electron micrographs (SEM) were collected on a JSM-7600F microscope from JEOL under high vacuum with an acceleration voltage of 2.0 kV. FRAP experiments were performed on an Eclipse Ti confocal microscope from Nikon Instruments, with a Yokogawa confocal spinning disk unit operated at 10,000 rpm, equipped with a Plan Fluor objective, and recorded with an Andor iXon Ultra 897 high speed EM-CCD camera. Human primary articular chondrocytes (hPACs) were counted on NucleoCounter NC-200 from ChemoMetec. Images for cell viability assessment in 3D cultures were captured on a LSM 710 confocal laser scanning microscope from Zeiss. Compressive mechanical loading of the 3D cell cultures was performed continuously in cycles on a MACH-1 mechanical tester from Biomomentum at RT. Confocal fluorescent images of

immunostained 3D cell cultures were acquired on a Stellaris 8 confocal laser scanning microscope from Leica with a supercontinuum white light laser (440-790 nm) and Power HyD detectors. Alcian Blue stained images were taken in brightfield on a light microscope from Olympus. The DNA concentration extracted from the hydrogels was measured on a NanoDrop from Thermo Scientific. A microplate reader from BioTek Synergy HT was used to quantitate sulfated glycosaminoglycan (s-GAGs) content through the dimethylmethylene blue (DMMB) assay using measured absorbance values at 525 and 595 nm. A benchtop LED light (~10 mW/cm², 375 nm) was employed to initiate crosslinking in all other samples except for the ones on the rheometer.

Hydrogel preparation

Preparation of supramolecular hydrogels (SN)

The preparation of the supramolecular hydrogels with different molar ratios of SQ-DT and SQ-RGD was executed according to an earlier published protocol[1b]. Briefly, SQ, SQ-DT and SQ-RGD stock solutions (10.0 mM) were prepared by adding dimethyl sulfoxide (DMSO) to each component with 2 min of vortexing. To acquire **SN** hydrogels with different total monomer concentrations or varied SQ-DT and SQ-RGD molar percentages, a pre-determined volume of the DMSO stock solutions containing the necessary components were pipetted into a glass vial (2 mL) followed by 30 s of gentle vortexing to obtain homogeneous solutions. The DMSO was then removed using a stream of N_2 overnight. Afterwards, the required volume of PBS was added to reach the desired concentration and sonicated in an ultrasonic ice-water bath for 10 to 30 min (0 °C - 4 °C) yielding a clear solution; the necessary sonication time depended on the monomer concentration and the power of sonication bath. The clear solutions were then incubated for 15 min in a 37 °C oven to form gels. The transparent **SN** hydrogels were further equilibrated at RT overnight and photopolymerized prior to other measurements. The **SN** hydrogel is composed largely of the native monomer SQ and SQ-DT and can include SQ-RGD depending on the experiment.

Preparation of PEG-based hydrogels (PN)

PEG-based polymeric hydrogels (**PN**) were prepared according to an earlier published protocol.[1a] The preparation of a **PN** with 3.6 wt% PEG network, containing 1.8 wt% PEGdiDT (6 kDa), 1.8 wt% PEGdiNB (6 kDa) and 1 mM photoinitiator lithium phenyl-2,4,6-trimethylbenzoylphosphinate (LAP) is used here as an example. First, stock solutions of PEGdiDT (3.9 wt%), PEGdiNB (3.9 wt%), and LAP (15 mM) were prepared separately by dissolving each component in PBS in a vial (2 mL) with 30 s of vortexing. Hereafter, PEGdiDT (70 µL), PEGdiNB (70 µL) and LAP (10 µL) stock solutions were pipetted into a new vial (2 mL) followed with another 30 s of vortexing to obtain a homogeneous precursor solution (150 µL). The volume ratio of PEGdiDT, PEGdiNB and LAP was always kept at 7:7:1 and were photopolymerized prior to other measurements.

Preparation of hybrid hydrogels (IPN and DN)

A simple one-pot strategy was used to prepare the **IPN** and **DN** hydrogels prior to photopolymerization. For example, to obtain the **IPN** (3.6 wt% **PN** and 5 mM **SN** (SQ)) and **DN** (3.6 wt% **PN** and 5 mM **SN** (SQ with 10 mol% SQ-DT)) hydrogels, pre-determined volumes of the PEG stock solutions (PEGdiDT: 3.9 wt%, PEGdiNB: 3.9 wt%) were dissolved in water, pipetted into (PEGdiDT: 70

µL and PEGdiNB: 70 µL) a new vial (2 mL) and gently pipetted up and down (10 times). The PEGdiDT/PEGdiNB solution was lyophilized overnight to obtain a white solid. Aliquots of PBS (20 µL) and LAP stock solutions (15mM, 10µL) were added to re-dissolve the above PEGdiDT/PEGdiNB solid. Then, the **SN** (120 µL, 6.25 mM (SQ) or 6.25 mM (SQ with 10 mol% SQ-DT)) after sonication in an ice bath was kept on ice and pipetted into the polymeric stock solution **PEG** (30 µL), followed by gentle pipetting up and down (10 times) to mix both polymers (150 µL). The obtained supramolecular and covalent polymer mixture was equilibrated at 37°C for 15 min to trigger supramolecular hydrogel formation and was stored at RT overnight. The preparation of all other **IPN** and **DN** hydrogels before photopolymerization followed this procedure. Finally, various UV exposure times (1 - 10 min) were used to crosslink the hybrid hydrogels (Figure S1). During this UV step, the covalent polymer network, and crosslinks in and with the supramolecular network are made simultaneously. Parameters such as total supramolecular monomer concentration, the molar percentage of SQ-DT in the supramolecular mixture, the total polymer concentration of PEGdiDT/PEGdiNB and UV exposure time were examined on the **DN** properties.

Table S1. Plateau storage moduli of the various hydrogels (**SN**, **PN**, **IPN** and **DN**) with different compositions (e.g., supramolecular monomer concentration, SQ-DT mol% in **SN**, total polymer concentration) and UV exposure times. Averaged storage moduli are presented (N ≥ 3).

System name	Composition				UV exposure time (min)	Storage modulus before UV exposure (Pa)	Storage modulus after UV exposure (Pa)
	SN (mM)	**SQ** (mol%)	**SQ-DT** (mol%)	**PEG** (wt%)			
SN	5.0	100	0	-	10	5 ± 1	8 ± 1
	5.0	99	1	-	10	9 ± 3	196 ±114
	5.0	95	5	-	10	44 ± 10	1392 ± 541
	5.0	90	10	-	10	91 ± 15	2816 ± 519
PN	-	-	-	1.8	10	S	VS
	-	-	-	2.4	10	S	177 ± 32
	-	-	-	3.6	10	S	1284 ± 56
IPN	5.0	100	-	1.8	10	VS	473 ± 118
	5.0	100	-	1.8	3	VS	239 ± 90
	5.0	100	-	2.4	10	VS	1093 ± 283
	5.0	100	-	3.6	10	VS	3704 ± 243
	5.0	100	-	3.6	3	VS	4193 ± 2351
DN	5.0	99	1	3.6	10	VS	7833 ± 583
	10.0	90	10	3.6	10	71 ± 2	11606 ± 553
	5.0	90	10	1.8	10	10 ± 8	3028 ± 129
	5.0	90	10	1.8	3	22 ± 9	2182 ± 350
	5.0	90	10	2.4	10	15 ± 12	4994 ± 370
	5.0	90	10	3.6	10	16 ± 7	10391 ± 541
	5.0	90	10	3.6	3	10 ± 5	9371 ± 213
	5.0	90	10	4.8	10	10 ± 10	11815 ± 351
	5.0	90	10	7.2	10	4 ± 2	17307 ± 4273
	5.0	90	10	9.6	10	VS	21072 ± 5071

[S]: Solution; [VS]: Viscous Solution.

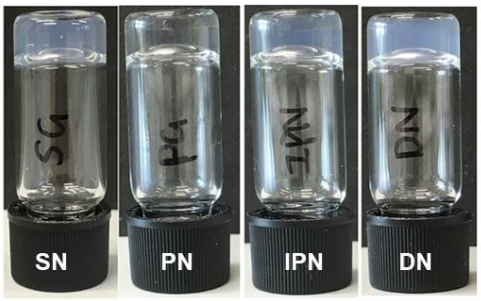

Figure S1. Gel inversion experiments of hydrogels after 3 min UV exposure using a LED at RT: **SN** (5 mM SQ with 10 mol% SQ-DT); **PN** (3.6 wt% PEG); **IPN** (3.6 wt% **PN** and 5 mM **SN** (SQ)); and **DN** (3.6 wt% **PN** and 5 mM **SN** (SQ with 10 mol% SQ-DT).

Oscillatory Rheology

The prepared hydrogels (**SN**, **IPN**, **DN**) (110 µL) and **PN** solutions (104 µL) prior to photopolymerization were gently pipetted on to the quartz plate of the rheometer. The upper plate was then lowered to a gap distance of 300 µm. The samples were then exposed to UV light for 10 min. Time sweeps (frequency = 1.0 Hz, strain = 0.05%), frequency sweeps from 0.01 to 10 Hz (strain = 0.05%), and strain sweeps from 0.01 to 1000% (frequency = 1.0 Hz) were collected. The self-recovery properties were measured using a step-strain experiment. After the above strain experiment, a time-dependent recovery measurement was applied at low strain (0.05%) for 300 s. Once the storage modulus reached its plateau, a high strain (500%) was applied for 300 s. The application of high- and low strain in an alternating fashion was repeated for two cycles. The recovery rate[2] of the hydrogels were calculated by collecting the storage modulus before (G_0') and after (G_t') the large strain was applied. The recovery rate (%) was determined as following: recovery rate (%) = (G_t'/G_0')*100%.

The strain stiffening behaviour of hydrogels with different UV exposure times were evaluated in the rheometer applying the pre-stress method. The hyhdrogels were subjected to a constant pre-stress (from 0.5 Pa) upon which a small oscillatory stress was superimposed, $\delta\sigma(t) = \delta\sigma e^{iwt}$, up to a maximum of 10% of the prestress at a fixed frequency (1.0 Hz). The stress relaxation behaviour of the hydrogels with different UV exposure times were measured at a constant strain of 10%. The stress (σ) was normalized to the average stress (σ_0) during the first two seconds at the beginning of data collection. The creep and recovery behavior of the hydrogels with different UV exposure times were performed after a time sweep of 1200 s with a fixed strain (0.01%) and frequency (1.0 Hz). The strain in response to a constant stress (1 Pa for **DN** hydrogel with 0 min UV exposure, 0.3 kPa for **DN** hydrogel with 1 min and 3 min photoirradiation) was measured for 3600 s, after which the stress was removed, and the strain was measured for another 5000 s. Water was added on top of the cover surrounding the upper plate to reduce drying of the hydrogels during the measurement.

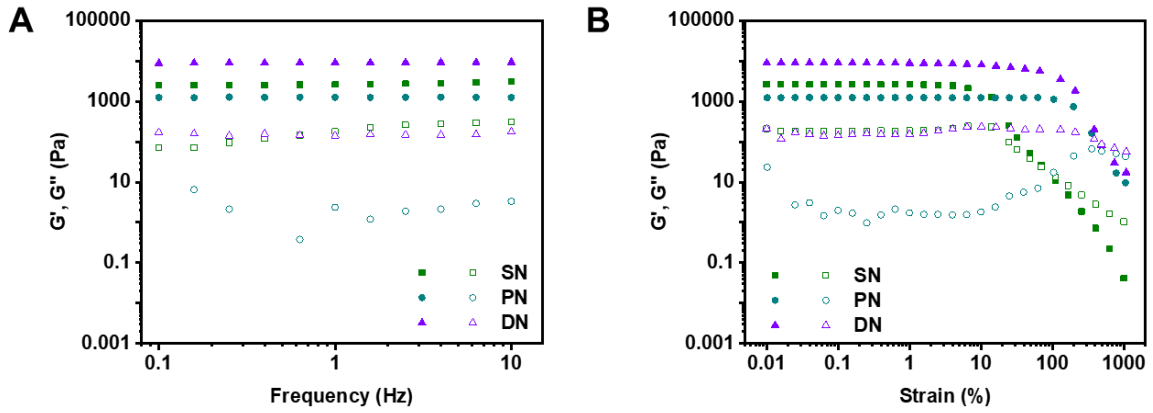

Figure S2. Averaged (N = 3) (A) frequency (0.1-10 Hz) and (B) strain (0.01-1000%) sweeps of hydrogels at RT: **SN** (5 mM (SQ with 10 mol% SQ-DT), **PN** (3.6 wt%) and **DN** (3.6 wt% **PN** network and 5 mM **SN** (SQ with 10% mol SQ-DT)). The frequency sweep experiment was performed at a fixed strain (0.05%) and the strain experiment was collected at fixed frequency (1.0 Hz).

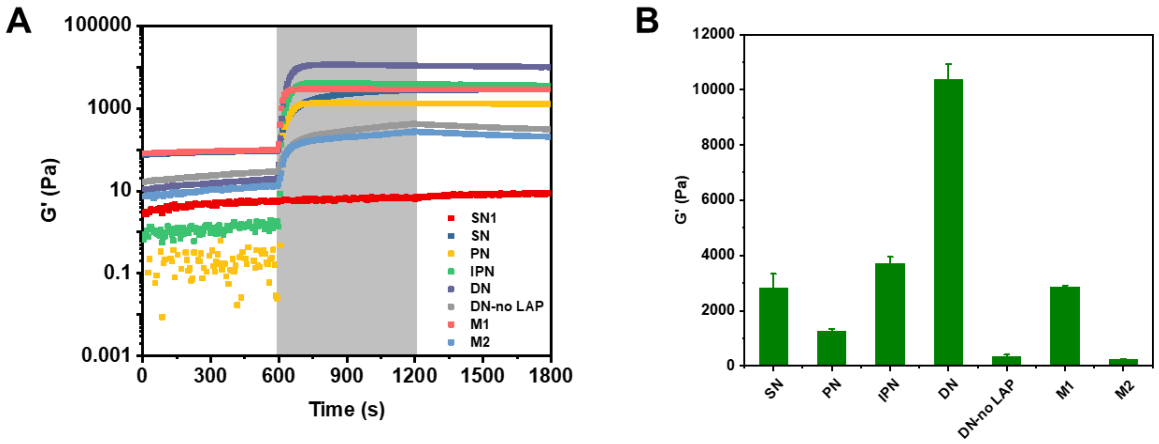

Figure S3. (A) Averaged (N = 3) time sweep experiment and (B) Plateau storage moduli of the various hydrogels after 10 min UV exposure measured at a fixed frequency (1.0 Hz) and strain (0.05%) at RT: (1) **SN** (5 mM (SQ with 10 mol% SQ-DT)); (2) **SN1** (5 mM SQ); (2) **PN** (3.6 wt%); (3) **IPN** (3.6 wt% **PN** network and 5 mM **SN** (SQ)); (4) **DN** (3.6 wt% **PN** network and 5 mM **SN** (SQ with 10 mol% SQ-DT)); (5) **DN-no LAP** (3.6 wt% **PN** network and 5 mM **SN** (SQ with 10 mol% SQ-DT)) (6) **M1** (5 mM **SN** (SQ with 10 mol% SQ-DT) and 1.8 wt% PEGdiNB with 1.0 mM LAP); and (7) **M2** (5 mM **SN** (SQ with 10 mol% SQ-DT) and 1.8 wt% PEGdiDT with 1.0 mM LAP). Grey regions indicate UV exposure. The standard deviation was calculated according to the average of repeat independent measurements (N ≥

3).

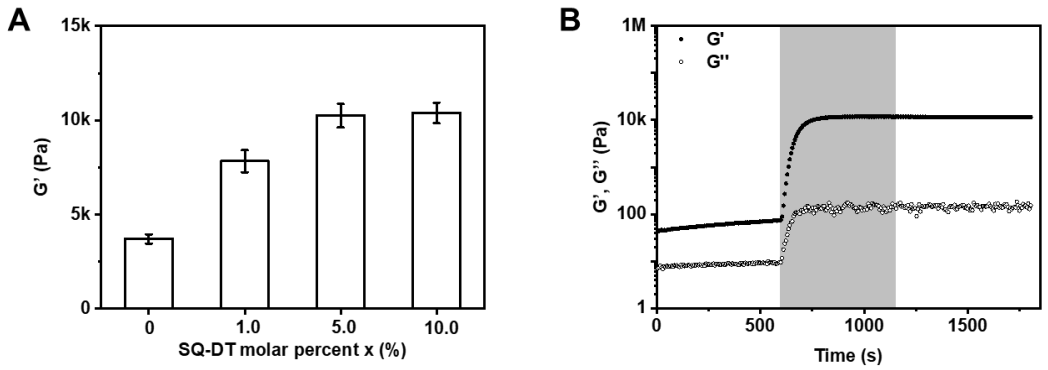

Figure S4. (A) Plateau storage moduli of **DN** (3.6 wt% **PN** network and 5 mM **SN** (SQ with 0-10 mol% SQ-DT)), (B) Averaged (N = 2) time sweep experiment of **DN** (3.6 wt% **PN** network and 10 mM **SN** with 5 mol% SQ-DT) with 10 min UV exposure. The measurement was performed under fixed frequency (1.0 Hz) and strain (0.05%). Grey regions indicate UV exposure. The standard deviation was calculated according to the average of repeat independent measurements (N ≥ 3).

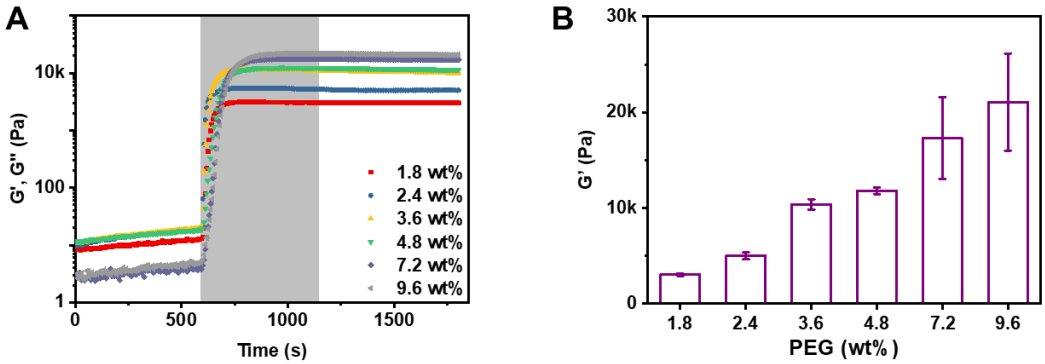

Figure S5. (A) Averaged (N = 3) time sweep experiment and (B) the plateau storage moduli of various **DN** with 5 mM **SN** (SQ with 10 mol% SQ-DT) and different **PN** concentrations after 10 min UV exposure. The measurement was performed under fixed frequency (1.0 Hz) and strain (0.05%). Grey regions indicate UV exposure. The standard deviation was calculated according to the average of repeat independent measurements (N ≥ 3).

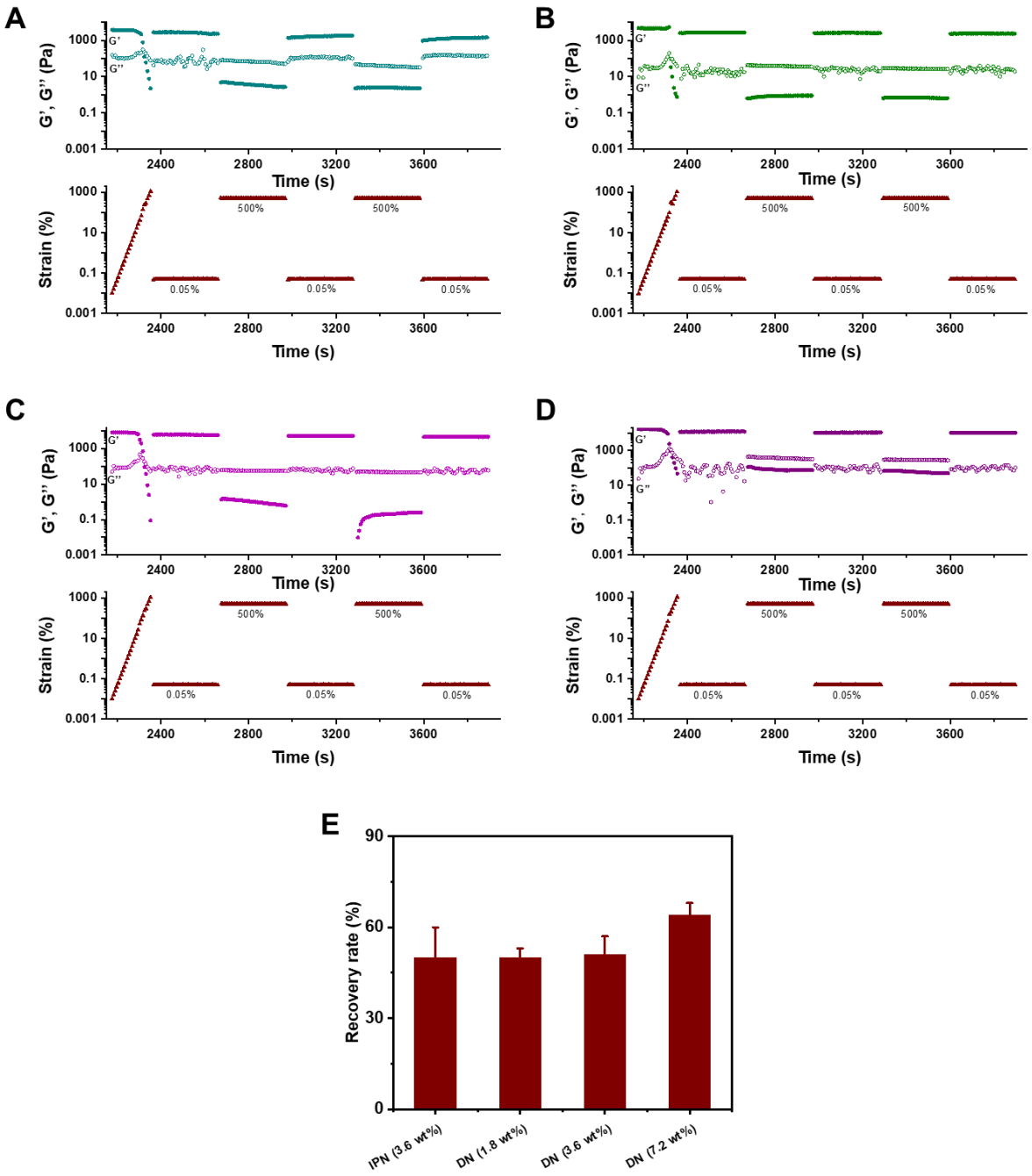

Figure S6. Averaged (N = 3) step-strain experiments of the various **IPN** and **DN** hydrogels: (A) **IPN** (3.6 wt% **PN** network and 5 mM **SN** (SQ)) (B) **DN** (1.8 wt% **PN** network and 5 mM **SN** (SQ with 10 mol% SQ-DT)). (C) **DN** (3.6 wt% **PN** network and 5 mM **SN** (SQ with 10 mol% SQ-DT)). (D) **DN** (7.2 wt% **PN** network and 5 mM **SN** (SQ with 10 mol% SQ-DT)) (E) The averaged (N = 3) storage recovery rate of **IPN** hydrogels (5 mM **SN** (SQ)) and various **DN** hydrogels (5 mM **SN** (SQ with 10 mol% SQ-DT) with different **PN** concentrations.

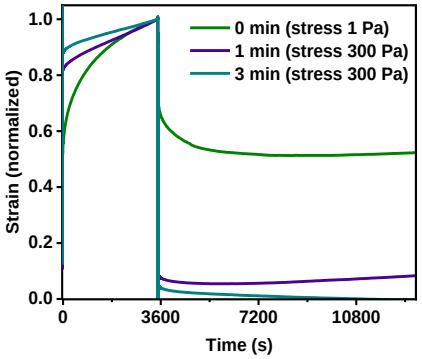

Figure S7. Creep and recovery test of **DN** (3.6 wt% **PN** network and 5 mM **SN** (SQ with 10 mol% SQ-DT) after different UV exposure times (0 min, 1 min and 3 min). A constant stress of 1 Pa was applied to the sample with 0 min UV exposure, whereas 0.3 kPa was applied to the samples with 1 min and 3 min.

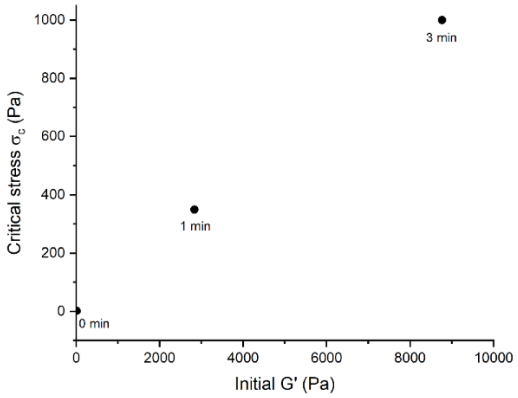

Figure S8. Critical stress (σ_c) as a function of initial storage modulus of **DN** hydrogels (3.6 wt% **PN** network and 5 mM **SN** (SQ with 10 mol% SQ-DT)) with various UV exposure times (0 min, 1 min and 3 min) at RT.

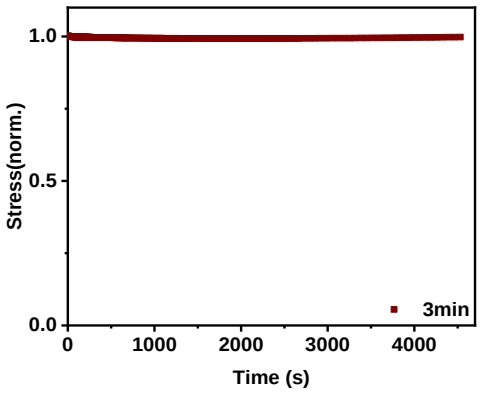

Figure S9. Stress relaxation behavior (10% strain) of the **PN** (7.2 wt%, 3 min).

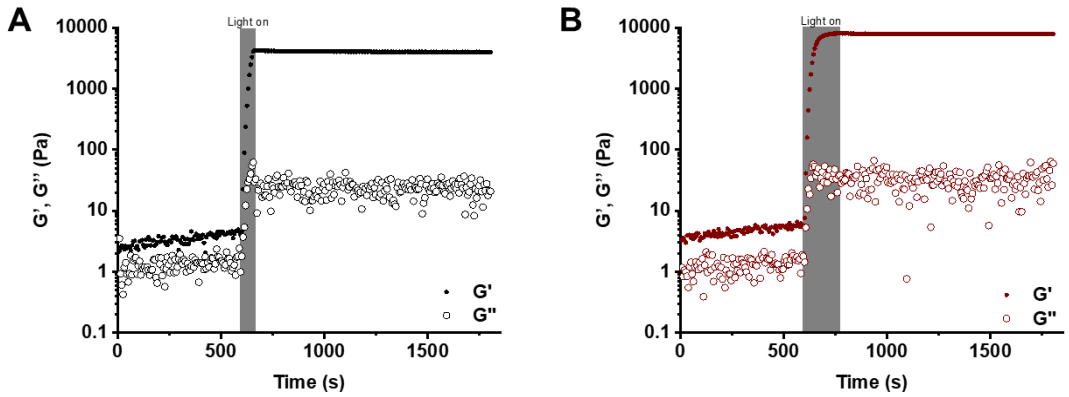

Figure S10. Averaged (N = 2) time sweep experiment of **DN** hydrogels (3.6 wt% **PN** network and 5 mM **SN** (SQ with 10 mol% SQ-DT and 5 mol% SQ-RGD)) with different UV exposure times measured at fixed frequency (1.0 Hz) and strain (0.05%) at RT: (A) 1 min and (B) 3 min. Grey regions indicate UV exposure.

Compression test

The prepared samples before photopolymerization (20 mm geometry: 400 µL; 8 mm geometry: 75 µL) were gently pipetted on to the quartz plate of the rheometer and the upper plate was lowered to 1.2 mm. The samples were equilibrated for 5 min before data collection. After a time sweep experiment of 60 s, the samples were UV exposed for 10 min to reach a plateau in storage modulus. PBS was carefully placed around the samples immediately after the samples were fully crosslinked to prevent evaporation during the measuring period. Afterwards, an axial compression test was set up to compress the sample ~80 % of its initial height (0.2 mm gap) at a rate of 10 µm/s. The compression modulus was calculated from the slope of the linear region of the compressive stress-strain curve (**SN**: strain = 0-2%, other samples: strain = 5-10%). Cyclic axial compression (loading and unloading) tests were performed on the UV exposed hydrogels by compressing them to 2% of their initial heights at a rate of 10 µm/s and then removing the load. The next compression cycle was started immediately after release of the load. Energy dissipation within the gels were probed under the same conditions as the cyclic axial compression test using increasing strain percentages from 5% to 50%. Compressive stress relaxation test on the UV exposed hydrogels were performed starting with applying 5% strain to the sample at a rate of 50 µm/s. The hydrogels were compressed for 10 min at this strain percentage and stress relaxation was monitored. Steps of 5% strain were then applied to the material in sequence for the same amount of time until a maximum of 20% strain was achieved. The curves were plotted until the hydrogel fractured.

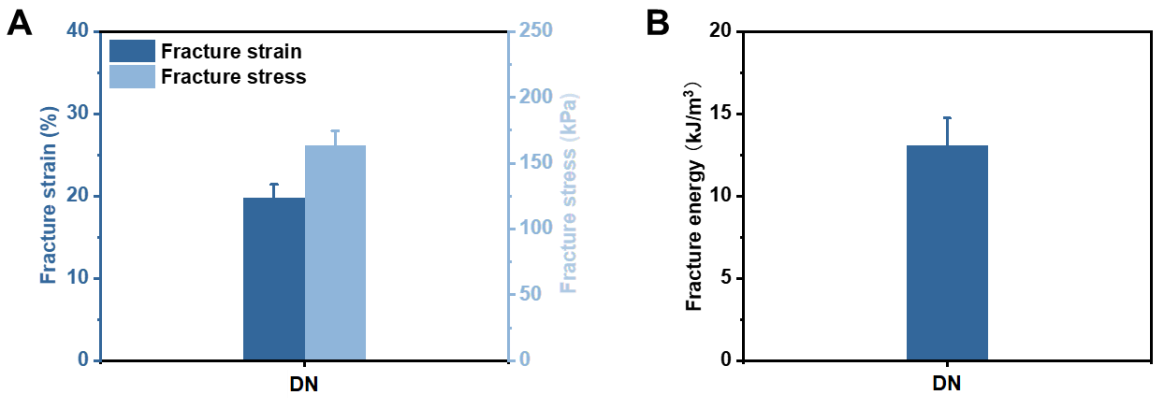

Figure S11. Mechanical properties of **DN** (3.6 wt% **PN** and 5 mM **SN** (SQ with 10 mol% SQ-DT) at fracture: (A) Compressive fracture strain and compressive fracture stress, (B) Fracture energy. The sample was compressed at a speed of 10 μm/s. Mean ± SD, N≥3.

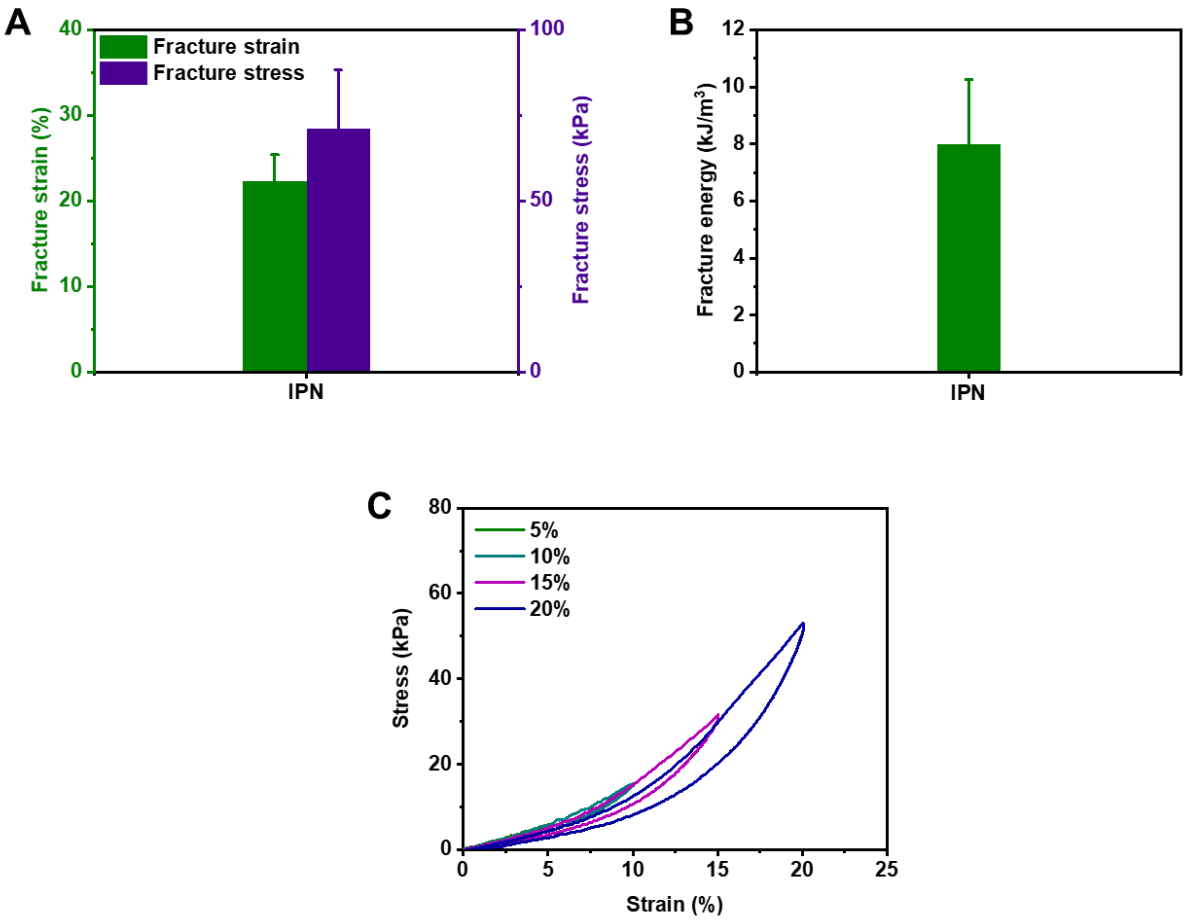

Figure S12. Mechanical properties of **IPN** hydrogels (3.6 wt% **PN** network and 5 mM **SN** (SQ)) at fracture: (A) Compressive fracture strain and compressive fracture stress, (B) Fracture energy. (C) Uniaxial compression cycles at different maximum strains. The sample was compressed at a speed of 10 μm/s. Mean ± SD, N≥3.

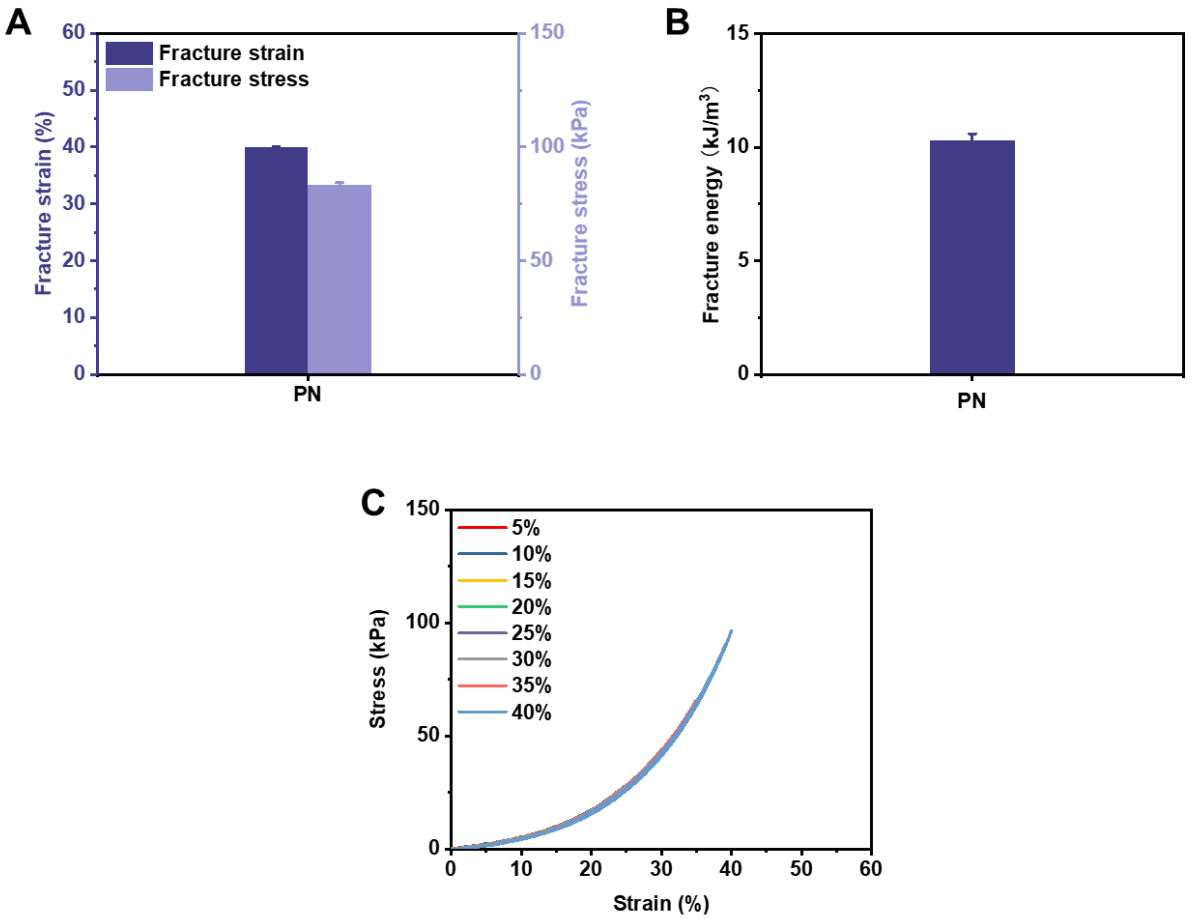

Figure S13. Mechanical properties of **PN** (3.6 wt% PEG) at fracture: (A) Compressive fracture strain and compressive fracture stress, (B) Fracture energy. (C) Uniaxial compression cycles at different maximum strains. The sample was compressed at a speed of 10 µm/s. Mean ± SD, N≥3.

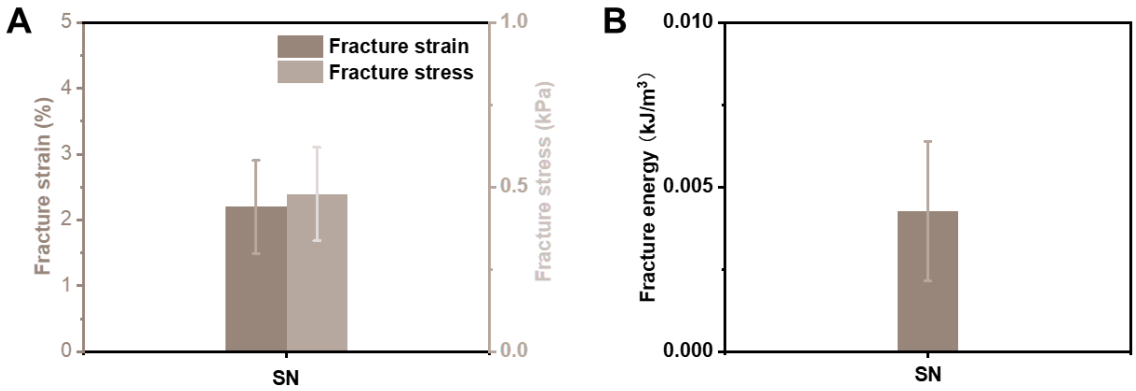

Figure S14. Mechanical properties of **SN** hydrogels (5 mM SQ with 10 mol% SQ-DT)) at fracture: (A) Compressive fracture strain and compressive fracture stress, (B) Fracture energy. The sample was compressed at a speed of 10 µm/s. Mean ± SD, N≥3.

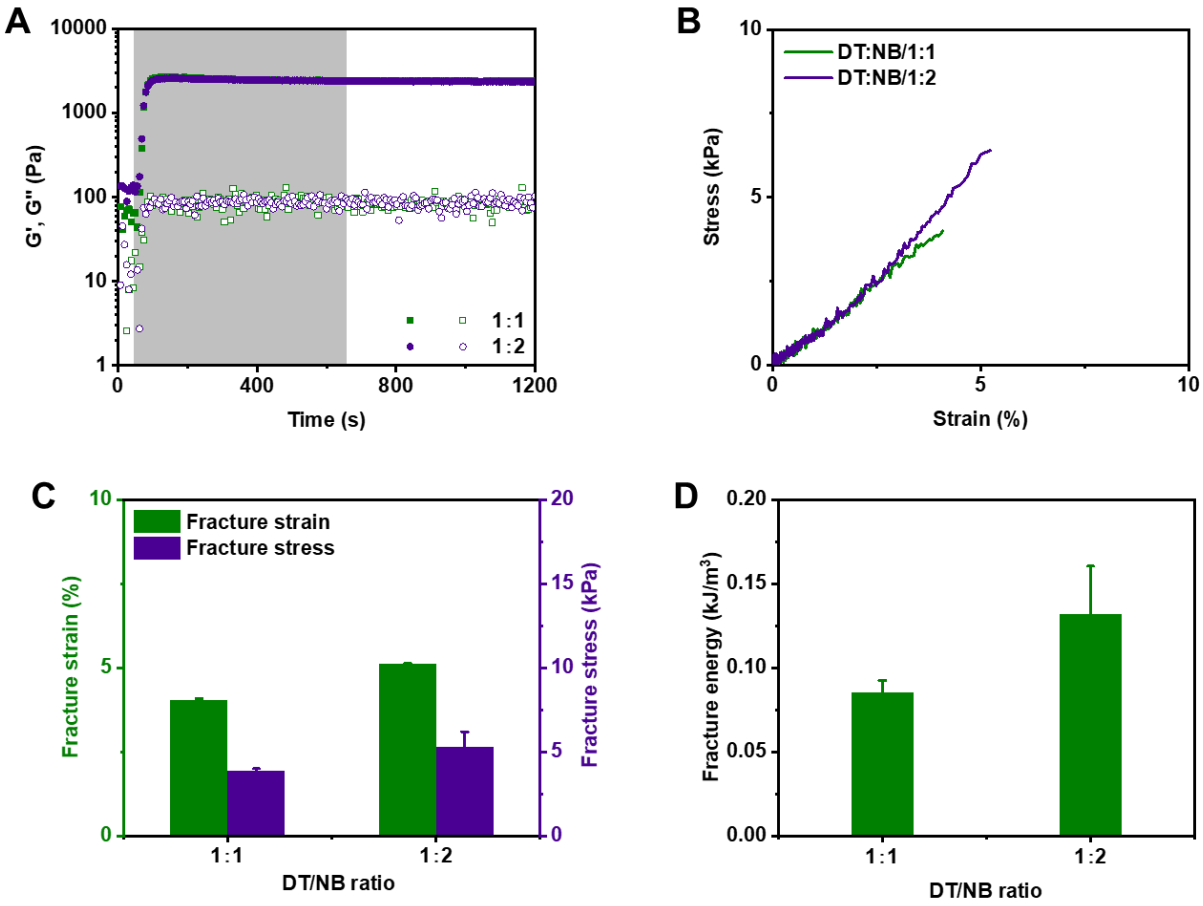

Figure S15. Mechanical properties of **SN** hydrogels **1:1** (5 mM **SN** (SQ with 10 mol% SQ-DT) and 0.45 wt% PEGdiNB, DT to NB molar ratio is 1:1) and **1:2** (5 mM **SN** (SQ with 10 mol% SQ-DT) and 0.9 wt% PEGdiNB, DT to NB molar ratio is 1:2). (A) Time sweep experiment after 10 min UV exposure. (B) Uniaxial stress-strain curves at a constant compression speed (10 µm/s). (C) Compressive fracture strain, fracture stress and (D) fracture energy. The sample was compressed at a speed of 10 µm/s. Mean ± SD, N≥3.

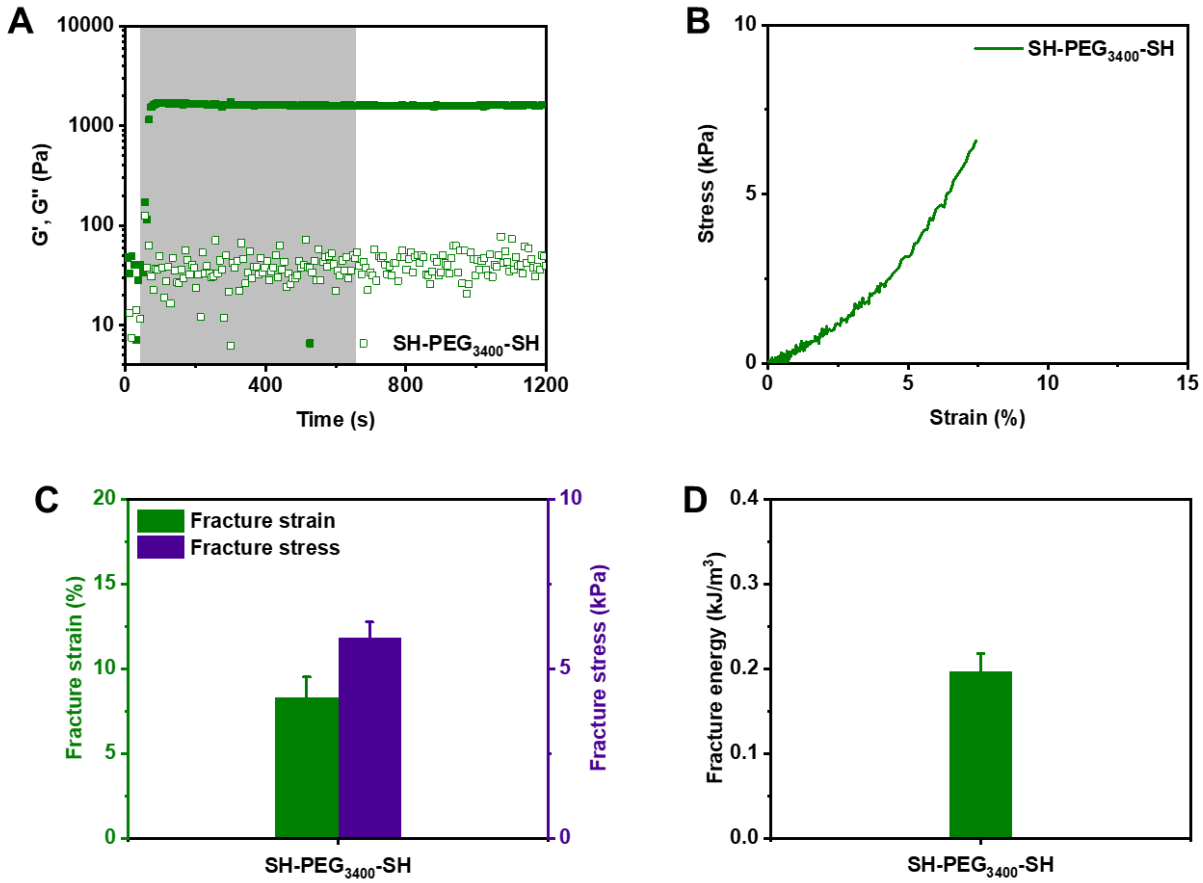

Figure S16. Mechanical properties of **DN** (5 mM **SN** (SQ with 10 mol% SQ-DT), and 1.8 wt% PEGdiNB and 1.0 wt% SH-PEG3400-SH). (A) Time sweep experiment of **DN** after 10 min UV exposure. (B) Uniaxial stress-strain curves under a constant compression speed (10 μm/s). (C) Compressive fracture strain, fracture stress and (D) fracture energy. The sample was compressed at a speed of 10 μm/s. Mean ± SD, N≥3.

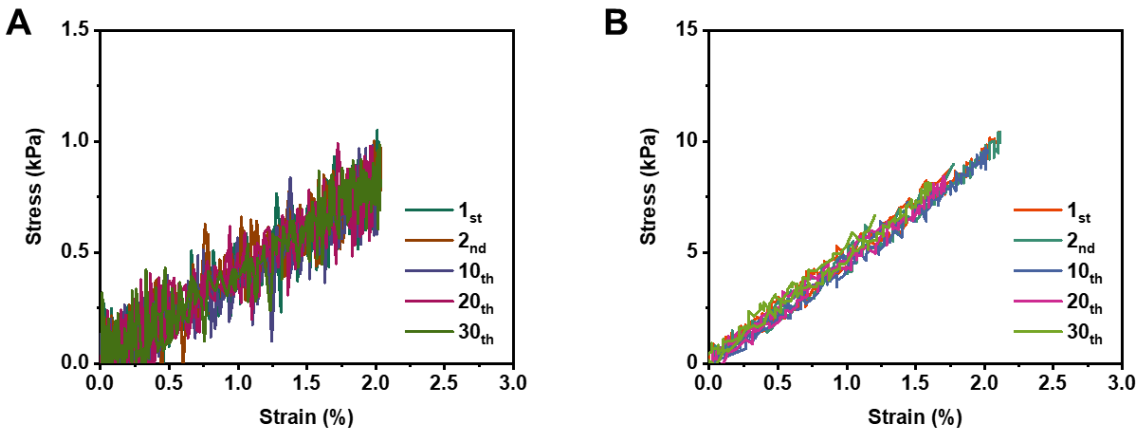

Figure S17. Representative loading-unloading curves of (A) **PN** (3.6 wt%) and (B) **DN** (3.6 wt% **PN** network and 5 mM **SN** (SQ with 10 mol% SQ-DT)). A strain of 2% was applied at a constant compression speed (10 μm/s).

Table S2. Fracture strain and stress, fracture energy, compression modulus and stress relaxation extent (axial) of the various hydrogels **SN**, **PN**, **IPN** and **DN** after 10 min UV exposure. (N ≥ 3).

Sample name	Fracture strain (%)	Fracture stress (kPa)	Fracture energy (kJ/m^3)	Compression modulus (kPa)	Stress relaxation extent (axial)
SN	2.20 ± 0.71	0.48 ± 0.14	0.00427 ± 0.00006	21.46 ± 5	/
PN	39.92 ± 0.11	83.52 ± 0.74	10.32 ± 0.2687	42.2 ± 8.4	~0
IPN	22.28 ± 3.09	71.10 ± 17.07	8.00 ± 2.26	216.01 ± 7.14	44% - 46%
DN	19.82 ± 1.59	163.66 ± 10.75	13.10 ± 1.65	360.61 ± 20.9	36% – 48%

SN: SQ with 10 mol% SQ-DT. **PN:** 3.6 wt%. **IPN:** 3.6 wt% **PN** and 5 mM **SN** (SQ with 10 mol% SQ-DT). **DN**: 3.6 wt% **PN** network and 5 mM **SN** (SQ with 10 mol% SQ-DT).

Cryogenic transmission electron microscopy (Cryo-TEM)

The **DN** samples prior to UV exposure were prepared as described above.[1b] The **DN** (3 µL) was applied to a freshly glow-discharged carbon 200 mesh Cu grid (Lacey carbon film) and the excess liquid was blotted off (3 s) at 100% humidity and plunge-frozen in liquid ethane prior to imaging.

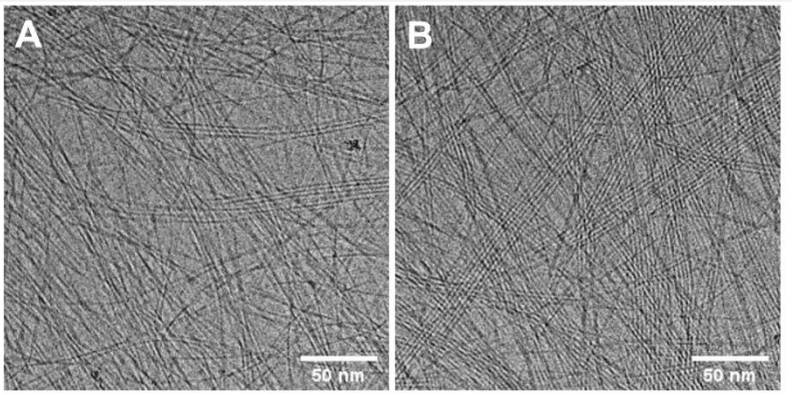

Figure S18. Cryo-TEM images of the **DN** with 5 mM **SN** (SQ with 10 mol% SQ-DT) and increasing **PN** concentration: (A) 3.6 wt% **PN** (B) 7.2 wt% **PN** without UV exposure. Scale bar: *50 nm*.

Scanning electron microscopy (SEM)

The **PN**, **IPN** and **DN** hydrogels (300 µL) were prepared as described above and exposed to UV light for 3 min by LED. The hydrogels were subsequently freeze-dried overnight and then, fractured after briefly dipping the solids in liquid nitrogen using tweezers. The fractured pieces were directly applied on to two-sided adhesive tape attached to an aluminum stub and coated for 2 min by a thin layer of gold (under vacuum) before imaging.

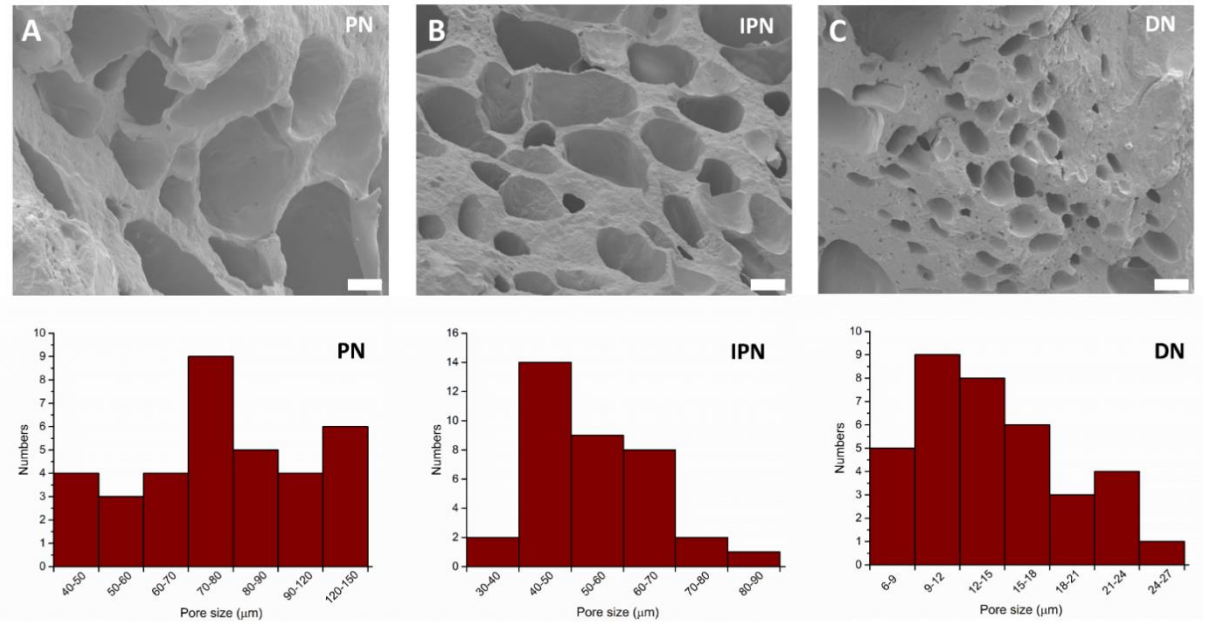

Figure S19. SEM images of the various hydrogels (A) **PN** (3.6 wt%), (B) **IPN** hydrogel (3.6 wt% **PN** and 5 mM **SN** (SQ with 10 mol% SQ-DT); (C) **DN** hydrogel (3.6 wt% **PN** network and 5 mM **SN** (SQ with 10 mol% SQ-DT)) and the relative distribution of measured pore sizes by the Image J software. Scale bar: *20 μm*.

Fluorescence recovery after photobleaching (FRAP) diffusion measurements

The hydrogel-fluorophore mixtures were prepared as previously described.[1b] The **SN** and **PN** mixtures were independently mixed prior to UV exposure with stock solutions of fluoresceinamine (Mw: 347 Da, 1.0 mM), FITC-dextran (Mw: ~10 kDa, 0.5 mM), and FITC-dextran (Mw: ~70 kDa, 0.15 mM) in PBS in a volume ratio of 9:1 (gel:fluorophore/fluorophore-labelled dextran). The hydrogel-fluorophore mixtures contained **DN** hydrogel (3.6 wt% **PN** network and 5 mM **SN** (SQ with 10% mol% SQ-DT) with either fluoresceinamine (347 Da, 100 µM), FITC-dextran (10 kDa, 50 µM), or FITC-dextran (70 kDa, 15 µM). Then, the mixtures (12 µL) were gently pipetted into a µ-Slide 15 well plate and were UV exposed for different durations (0 min, and 3 min) using a benchtop LED source (~10 mW/cm^2, 375 nm). The control **PN** (7.2 wt%) with either fluoresceinamine (347 Da, 100 µM), FITC-dextran (10 kDa, 50 µM), or FITC-dextran (70 kDa, 15 µM) was prepared following the same procedure above. The PEG-fluorophore hydrogel mixtures were exposed to UV light for 3 min using a benchtop LED source (~10 mW/cm^2, 375 nm). A well plate containing the various hydrogel-fluorophore mixtures were then loaded on a confocal microscope and samples were recorded with an Andor iXon Ultra 897 high speed EM-CCD camera to obtain 512 x 512 images with a resolution of 0.33 µm/pix using a 40x NA 0.8 plan fluor objective lens from Nikon. Prior to bleaching, the hydrogel-fluorophore mixtures were imaged for 2s with a 40 ms framerate. Then, a circular bleaching ROI (r = 12 µm), 40 µm into the hydrogel, was excited for 5 seconds (2 ms/pix dwell time) using a 488 nm Argon laser through an Andor FRAPPA unit. After bleaching, recovery images were recorded with a frame rate of 40 ms. All imaging was done at low laser excitation (1-10% of maximum intensity) to prevent bleaching and reference ROIs were used to normalize the recorded intensities at the bleaching spot.

Diffusion measurement

Figure S20A-B shows example recovery signals recorded for the hydrogel mixtures with fluoresceinamine (*light-grey*), 10 kDa FITC-dextran (*grey*) and 70 kDa FITC-dextran (*dark-grey*). The intensities were normalized by:

$$f_r(t) = \frac{f_{ROI}(t)/f_{ref}(t) - f_{ROI}(0)/f_{ref}(0)}{f_{ROI}(\infty)/f_{ref}(\infty) - f_{ROI}(0)/f_{ref}(0)}$$

Here $f_r(t)$ is the recovery signal, $f_{ROI}(t)$ the intensity of the bleached region and $f_{ref}(t)$ the intensity of the ROI, following Liu et al.[6] The recovery curves are well fit by a single exponential:

$$f_r(t) = A\left(1 - e^{-\frac{t}{t_0}}\right)$$

where t_0 can be used to determine the half-time of recovery by . . The averaged (n > 5) half times show that cell-culture associated biomolecules, like nutrients and growth factors, can adequately diffuse through the hydrogel.

Next to extracting the half-time of recovery, the diffusion constant was estimated by fitting the normalized recovery curves to:

$$f(t) = \sum_{n=0}^{\infty} \frac{-K^n}{n!} \frac{1}{1 + n\left[1 + \left(\frac{2t}{\tau_D}\right)\right]}$$

where τ_D is the 2-D characteristic diffusion time and K is the bleaching constant that depends on the experimental system.[7] For a Gaussian laser beam the diffusion constant is related to τ_D by $D = \omega^2/4\tau_D$, where ω is half the width of Gaussian laser profile determined at e^{-2} of the profile height. The radius was determined by fitting a Gaussian to the bleach spot (identical settings and depth to supramolecular hydrogels) of dried-out agar (2%)-fluoresceinamine (100 µM) samples and found to be $\omega = 17.1 \pm 1.6$. The diffusion constants are shown in **Table S3**. All calculations were performed in Matlab 2019a, using the curve-fitting and image-processing toolboxes.

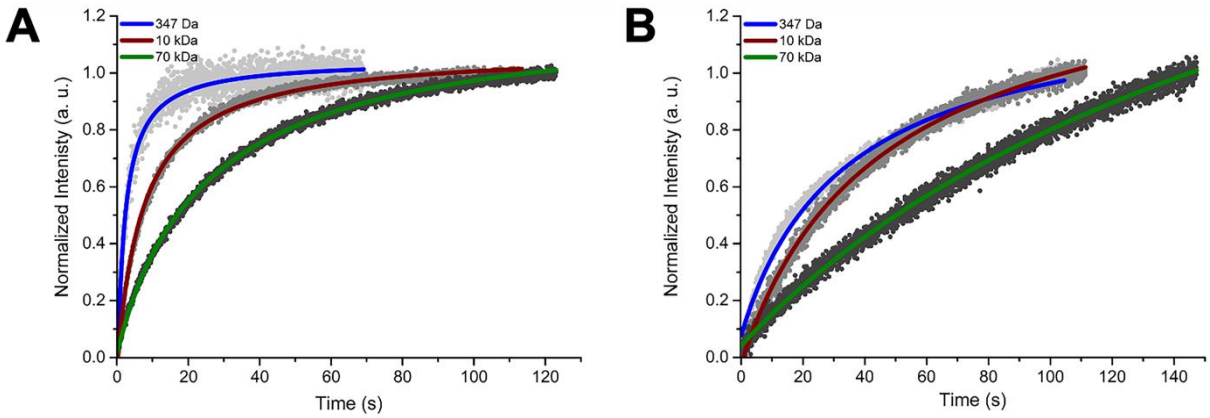

Figure S20. FRAP characterization of the **PN** and **DN** hydrogels with three different fluorescent probes (A) **DN** (3.6 wt% **PN** and 5 mM **SN** (SQ with 10 mol% SQ-DT)) without UV exposure and (B) **PN** (7.2 wt%) with 3 min UV exposure using different sized fluorophores (Fluoresceinamine (347 Da), and FITC-dextran (10 kDa and 70 kDa)). Grey dots: Normalized intensity in the bleached spot; Lines: fit of the diffusion constant.

Table S3. Effect of hydrogel composition and dye size on the diffusion coefficient (D) ($\mu m^2/s$).

Hydrogel composition	UV exposure time (min)	Fluorophore dye size 347 Da	10 kDa	70 kDa
DN (3.6 wt% **PN** network and 5 mM **SN** (SQ with 10 mol% SQ-DT))	0	23.66 ± 5.40	6.49 ± 1.48	2.01 ± 0.46
DN (3.6 wt% **PN** network and 5 mM **SN** (SQ with 10 mol% SQ-DT))	3	5.12 ± 1.17	3.52 ± 0.80	0.73 ± 0.17
PN (7.2 wt%)	3	1.57 ± 0.36	1.10 ± 0.25	0.18 ± 0.04

Equilibrium water content (EWC)

DN hydrogels (150 µL) were prepared in a glass vial (2.0 mL) as previously described and exposed to UV light for 3 min. To determine the equilibrium water content (EWC), they were first allowed to swell in PBS (600 µL) at 37 °C in an incubator for 24 h to reach equilibrium. Prior to measuring the hydrogel weight (W_s), the excess PBS was removed with a micropipet and blotted with a soft tissue paper. The hydrogels were then lyophilized overnight, and the weight was recorded (W_d). For all samples, three independent replicate experiments were performed. The EWC for each hydrogel was calculated using: EWC (%) = $(W_s-W_d)/W_s*100\%$.

Swelling and degradation assays

The swelling percentage of hydrogels were determined according to a previously published method.[3] Individual hydrogels (150 µL) were first prepared in a glass vial (2.0 mL) as described above and exposed to UV light for 3 min. The original weight (W_0) of each hydrogel prior to swelling was measured. Subsequently, each hydrogel was covered either with PBS or DMEM (high glucose) (600 µL), and then incubated at 37 °C. The weight (W_t) of all hydrogels was then collected at pre-determined time points, after complete removal of PBS or DMEM from the surface. The fresh PBS and DMEM were changed every two days during swelling. Three independent replicates were performed for each hydrogel condition. The swelling ratio was determined as $100\% * W_t/W_0$.

hPAC culture

Collection and expansion of hPACs from the ongoing Research Arthritis and Articular Cartilage (RAAK) study was performed as earlier described.[4] In short, within 2 hours following joint replacement surgery of osteoarthritis patients, cartilage of the macroscopically unaffected (preserved) region of the joint was sampled in DMEM (high glucose) supplemented with 10% FBS, antibiotics penicillin (100 units/mL) and streptomycin (100 µg/mL) and collagenase Type I (2 mg/mL); and were incubated overnight under standard conditions. Subsequently, isolated chondrocytes were expanded for 2 passages in DMEM supplemented with 10% FBS, antibiotics (100 units/mL penicillin and 100 µg/mL streptomycin) and FGF-2 (0.5 ng/mL) prior to encapsulation into the hydrogel materials.

3D cell encapsulation

3D cell encapsulation of hPACs in the **DN** (3.6 wt% **PN** network and 5 mM **SN** (SQ with 10 mol% SQ-DT without and with 5 mol% SQ-RGD) was explored. The hPAC suspension in the hydrogels were seeded at a density of 5 x 10^6 cells/mL. Different UV exposure times (0 min, 0.5 min, 1 min, and 3 min) were applied using a benchtop LED to crosslink the hydrogels and yield different mechanical properties. Afterwards, 3D constructs were covered with chondrogenic differentiation medium (500 µL) (DMEM high glucose supplemented with ascorbate (50 µg/mL), Dexamethasone (0.1 µM), L-proline (40 µg/mL), sodium pyruvate (100 µg/mL), ITS-plus, antibiotics, and TGF-β1 (10 ng/mL) and cultured under standard conditions. Cell media was refreshed 3 times every 15 min after seeding and was changed daily during the experiment.

Cell viability test

The LIVE/DEAD (calcein AM/propidium iodide (PI)) assay was used to assess cell viability after 3D encapsulation of the cells within the hydrogel. The mixed staining solutions of calcein AM (2.0 µM) and PI (1.5 µM) were prepared by diluting pre-prepared stock solutions of calcein AM (2.5 mM in DMSO) and PI (1.5 mM in PBS) with PBS (pH 7.4). At pre-determined time points (e.g., day 1 and 5), the medium was removed from the top of the hydrogel, the cell-laden hydrogels were washed with PBS (2 x 48 µL). The hydrogel was covered with the staining solution (48 µL) for 30 min at 37 °C and then removed from the top of hydrogel, and further washed with PBS (2 x 48 µL). An additional volume of PBS (48 µL) was pipetted on top of the hydrogel to prevent drying during imaging. Fluorescent Z-stack images were obtained using a 488 nm laser for excitation of calcein AM and a 532 nm laser for excitation of the PI dye. The Image J software package was used to process the collected raw images and count cell viability. LIVE/DEAD staining of hPACs was performed after 1 day and 5 days culture within hydrogels.

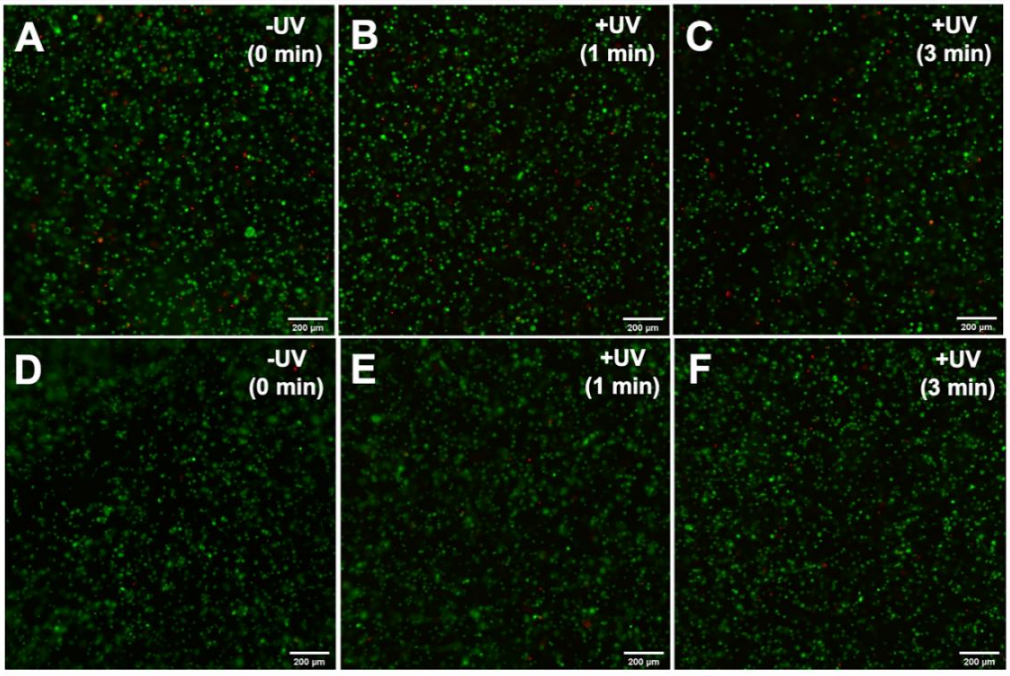

Figure S21. Confocal microscopy images of calcein AM/PI stained hPACs cells after culture day 1 in the **DN** hydrogels (3.6 wt% **PN** and 5 mM **SN** (SQ with 10 mol% SQ-DT without and with 5 mol% SQ-RGD) and different UV exposure times: (1) **DN**

without SQ-RGD at (A) 0 min; (B) 1 min; (C) 3 min; (2) **DN** with 5 mol% SQ-RGD at (D) 0 min; (E) 1 min; (F) 3 min. Viable cells are green and dead cells are red. Scale bar: *200 μm*.

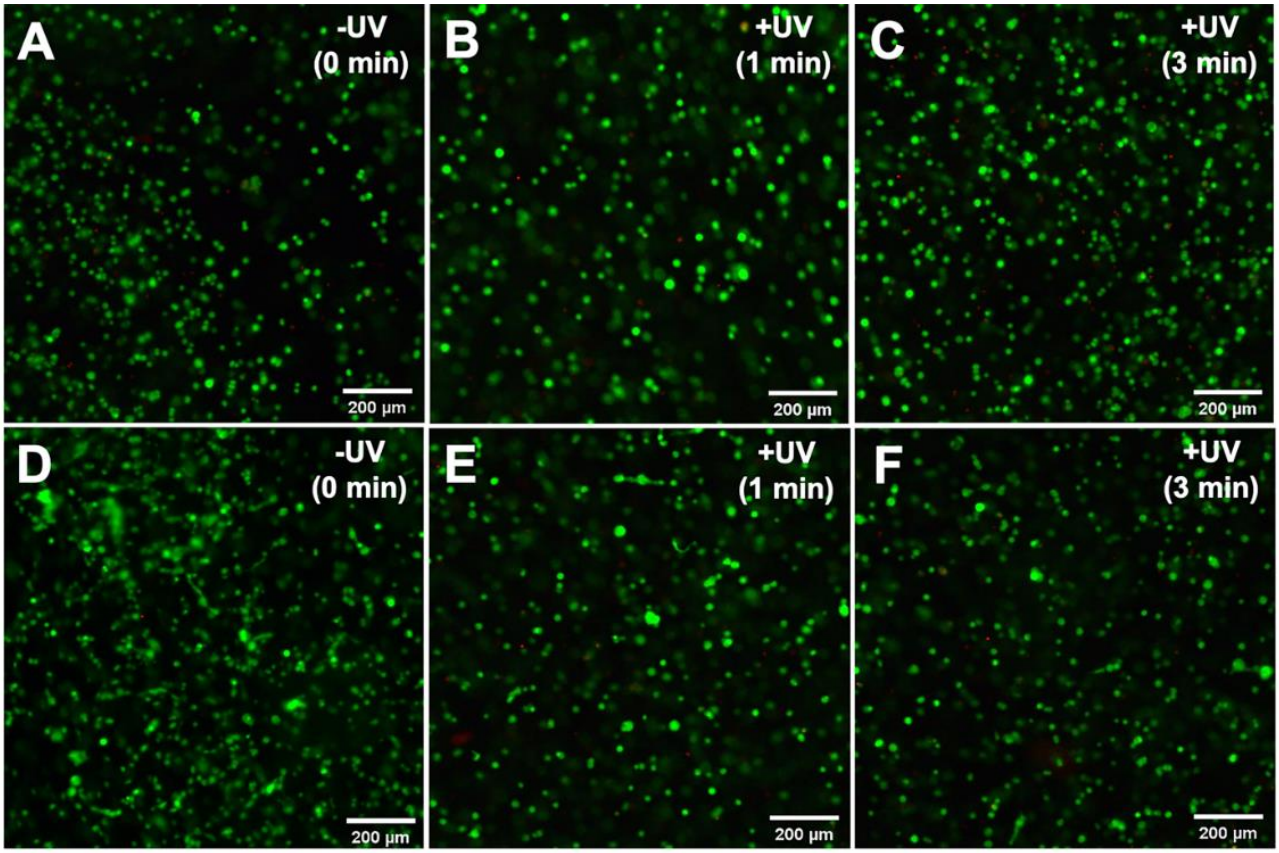

Figure S22. Confocal microscopy images of calcein AM/PI stained hPACs cells after culture day 5 in the **DN** hydrogels (3.6 wt% **PN** and 5 mM **SN** (SQ with 10 mol% SQ-DT without and with 5 mol% SQ-RGD) and different UV exposure times: (1) **DN** without SQ-RGD at (A) 0 min; (B) 1 min; (C) 3 min; (2) **DN** with 5 mol% SQ-RGD at (D) 0 min; (E) 1 min; (F) 3 min. Viable cells are green and dead cells are red. Scale bar: *200 μm*.

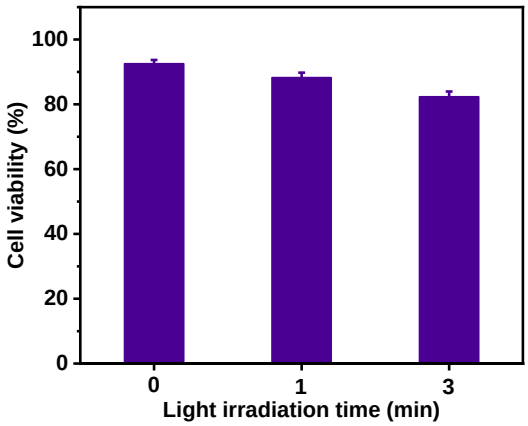

Figure S23. LIVE/DEAD counting of cells after 3D encapsulation of hPACs cell viability in **DN** hydrogels (3.6 wt% **PN** network and 5 mM **SN** (SQ with 10 mol% SQ-DT) with distinct UV exposure after 24h.

Compressive loading in 3D cell culture

Agarose culture wells with a diameter of 4 mm and a height of 1 mm were prepared by putting agarose (350 µL, 3%) in each well of a 24-well flat-bottom plate, using a 4 mm metal punch to create a small hole in the middle of the solidified agarose. The cell-laden hydrogel **DN** (20 µL) before UV exposure was gently pipetted into agarose wells. Then the cell-laden constructs were UV exposed (3 min) using a benchtop LED. Chondrogenic differentiation media (500 µL) with TGF-β1 (10 ng/ml) was carefully pipetted on top of construct. The plate was cultured under standard cell culture conditions. Cell media was refreshed 3 times every 15 min after seeding and was changed daily during the experiment.

For short-term (2 days) loading, the cell culture medium was carefully removed from the culture plate and the hydrogels were washed once with PBS before covering with the same buffer. The hydrogels were mechanically loaded independently for 10 minutes with a strain amplitude of 2% and fixed frequency of 1.0 Hz as soft loading, and a larger strain (20%) amplitude at a higher frequency (5.0 Hz) as heavy loading. After loading, the hydrogels were covered with chondrogenic differentiation media and further cultured under standard cell culture conditions. The control hydrogels were placed at the RT for 10 min in PBS.

For long-term (14 days) loading, the cell-laden hydrogels were exposed following the conditions for soft loading (2% strain amplitude at a fixed frequency (1.0 Hz)) for 45 minutes each day. Compressive loads were applied on days 1-3, 6-10 and 13-14.

Alcian Blue staining

To perform Alcian Blue staining of sulphated glycosaminoglycans (s-GAGs), the hPACs encapsulated in hydrogels were first fixed by applying formaldehyde (4%) for 15 min at RT. The hydrogels were washed with PBS (3 x 500 µL) and incubated with HCl (0.1N, 500 µL) for 10 min. To detect s-GAGs, the hydrogels were incubated with Alcian Blue 8-GX (1%) in HCl (0.1N) for 3 h and with HCl (0.1N, 3 x 500 µL), followed by adding HCl (0.1N, 500 µL) and incubated at RT overnight to totally remove the excess Alcian Blue. The hydrogels were washed with Milli-Q water (3 x 500 µL) before adding Nuclear Fast Red (0.1% in 5% aluminum sulfate) to stain the cell nuclei and incubated for 10 min before washing with MilliQ water (3 x 500 µL) before imaging.

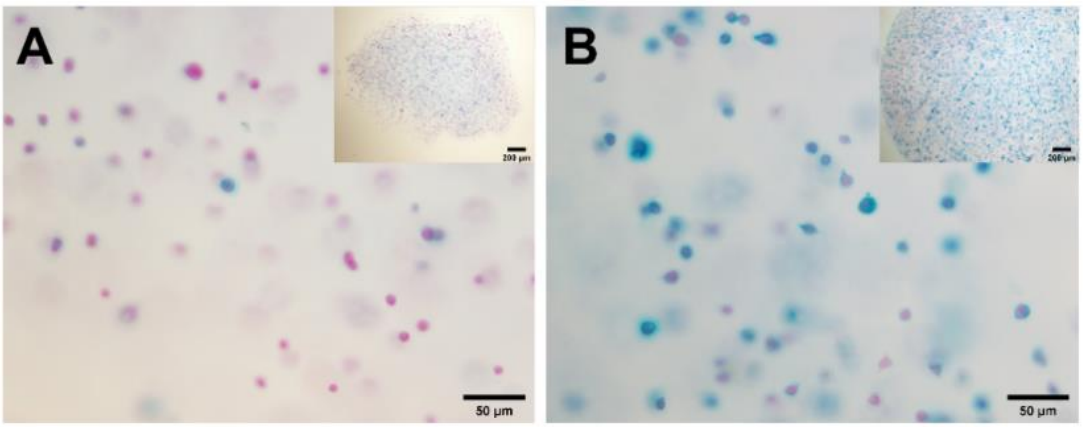

Figure S24. At day 5, Alcian Blue staining for s-GAGs with nuclear fast red counterstaining of hPACs in cell-laden **DN** hydrogels (7.2 wt% **PN** and 5 mM **SN** (SQ with 10 mol% SQ-DT) without SQ-RGD with UV exposure times: (A) 0 min and (B) 3 min. All cell-laden hydrogels were maintained in chondrogenic media containing TGF-β1.

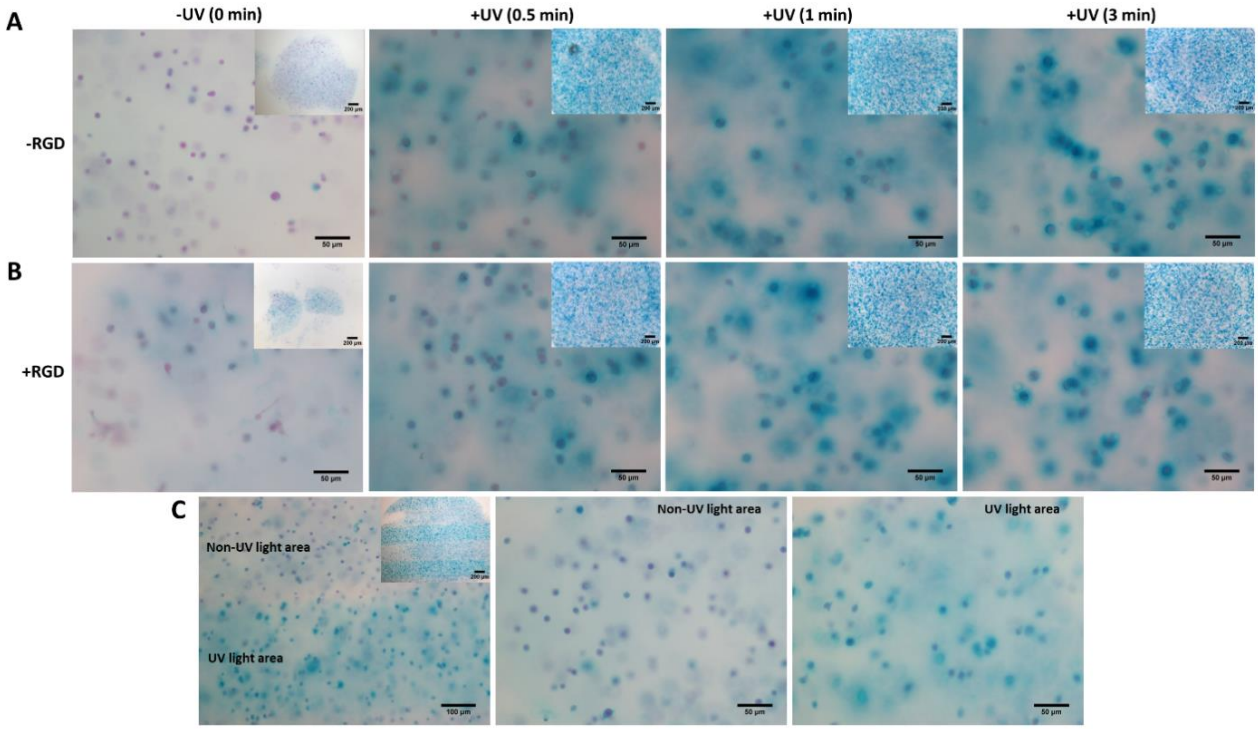

Figure S25. At day 5, Alcian Blue staining for s-GAGs with nuclear fast red counterstaining of hPACs in cell-laden hydrogels with varying UV exposure times (0 min, 0.5 min, 1 min and 3 min): (A) **DN** (3.6 wt% **PN** and 5 mM **SN** (SQ with 10% molar SQ-DT) without SQ-RGD and B) with 5 mol% SQ-RGD. (C) hPACs cell-laden **DN** hydrogels (3.6 wt% **PN** network and 5 mM **SN** with 10% mol SQ-DT) patterned with 3 min UV exposure using a photomask. All the cell laden hydrogels were maintained in chondrogenic media containing TGF-β1.

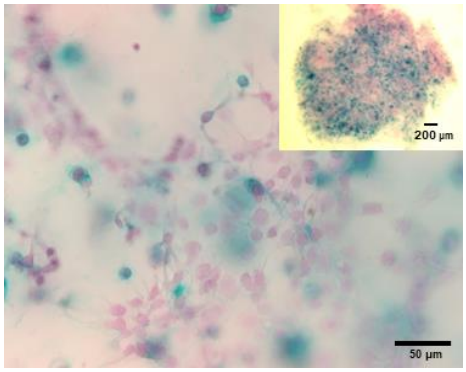

Figure S26. Representative Alcian Blue staining images with nuclear fast red counterstaining of hPACs cell-laden **DN** hydrogels (3.6 wt% **PN** and 5 mM **SN** (SQ with 10% mol SQ-DT and 5 mol% SQ-RGD)) without UV exposure and mechanical loading after culture day 3 in chondrogenic media containing TGF-β1.

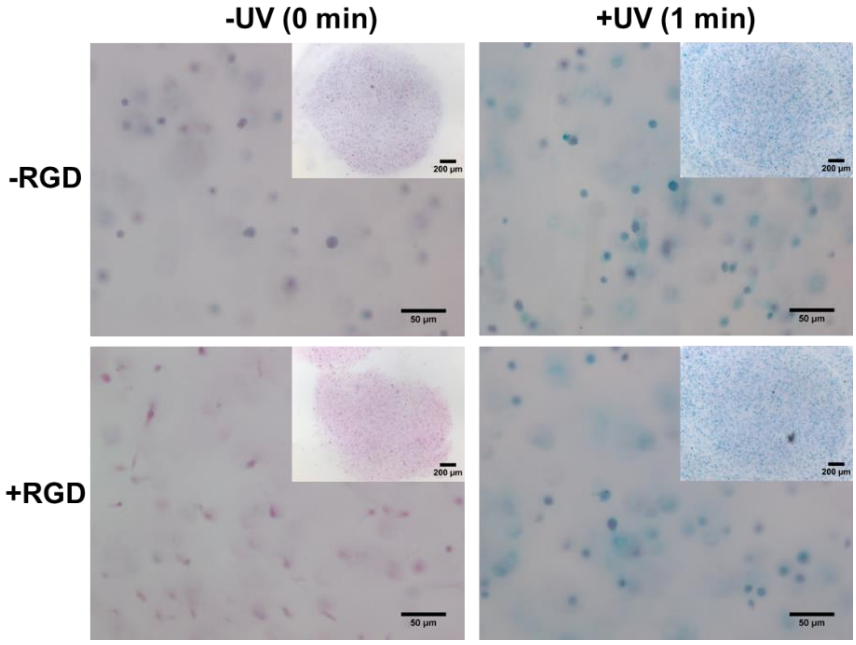

Figure S27. At day 5, Alcian Blue staining for s-GAGs with nuclear fast red counterstaining of hPACs in cell-laden **DN** hydrogels (3.6 wt% **PN** and 5 mM **SN** (SQ with 10 mol% SQ-DT) with/without 5 mol% SQ-RGD with varying UV exposure times (0 min, 1 min). All cell-laden hydrogels were maintained in chondrogenic media without TGF-β1.

DMMB assay and DNA content analysis

The s-GAGs and DNA content at indicated time points was quantified using biochemical analysis. The wet cell-hydrogel constructs were first weighed, lyophilized and digested overnight at 60 °C by a papain digestion solution in PBS-EDTA (pH 7.1). The s-GAGs concentration was measured by using DMMB assay[5] with Shark chondroitin sulfate in PBS-EDTA (pH 7.1) as a reference. The obtained solution was diluted 30x before performing measuring DMMB absorption at 525 and 595 nm. The concentration of DNA from the digested hydrogel samples were measured on a NanoDrop.

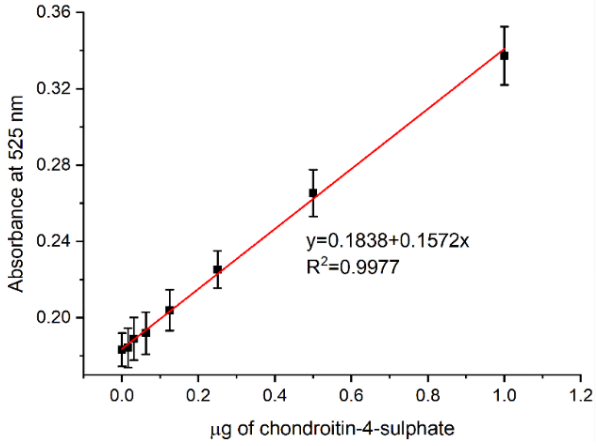

Figure S28. Standard solution curve for DMMB assay using chondroitin-4-sulfate.

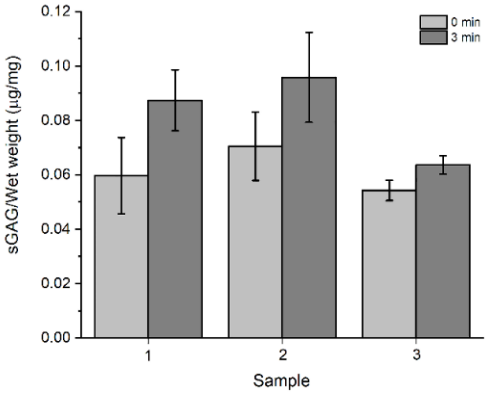

Figure S29. Results of the biochemical analysis of s-GAGs after 5 days culture of hPACs in cell-laden hydrogels with different UV exposure times (0 min and 3 min): sample 1: **DN** (3.6 wt% **PN** and 5 mM **SN** (SQ with 10 mol% SQ-DT)) without SQ-RGD. Sample 2: **DN** (3.6 wt% **PN** and 5 mM **SN** (SQ with 10 mol% SQ-DT)) with 5 mol% SQ-RGD. Sample 3: **DN** (7.2 wt% **PN** and 5 mM **SN** (SQ with 10 mol% SQ-DT)) without SQ-RGD. All cell laden hydrogels were maintained in chondrogenic media containing TGF-β1.

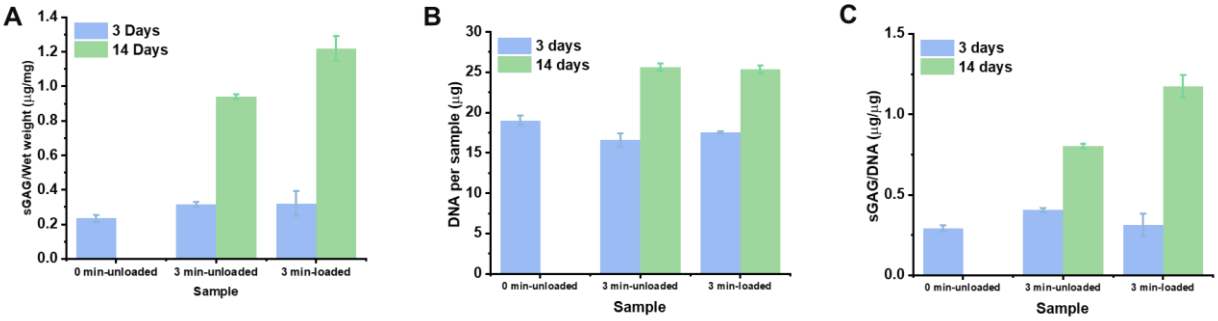

Figure S30. Results of biochemical analysis of s-GAGs, wet cell-laden hydrogel weight and DNA content after culture days 3 and 14 of hPACs (donor 1) in cell-laden **DN** hydrogels (3.6 wt% **PN** and 5 mM **SN** (SQ with 10 mol% SQ-DT and 5 mol% SQ-RGD)) and different UV exposure times (0 min and 3 min) and with/without mechanical loading (strain: 2%, frequency: 1Hz). (A) s-GAGs content normalized to wet cell-laden hydrogel weight. (B) Quantification of extracted DNA. (C) s-GAGs content normalized to the DNA content. All the cell laden hydrogels were maintained in chondrogenic media containing TGF-β1.

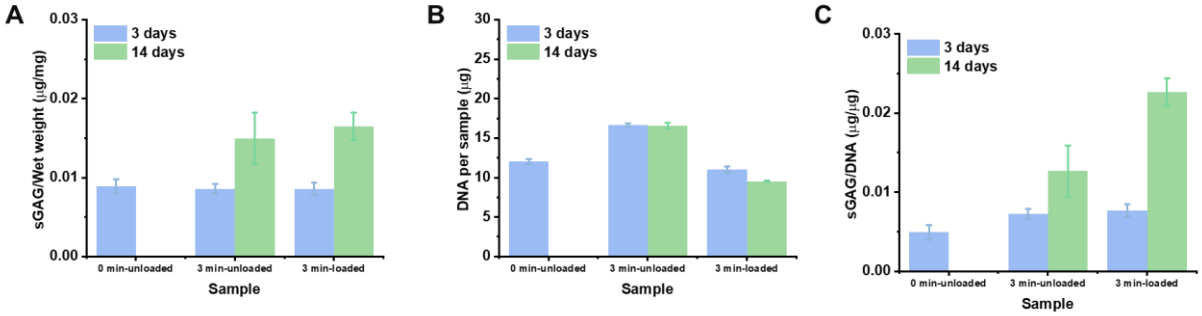

Figure S31. Results of biochemical analysis of s-GAGs, wet cell-laden hydrogel weight and DNA content after culture days 3 and 14 of hPACs (donor 2) in cell-laden **DN** hydrogels (3.6 wt% **PN** and 5 mM **SN** (SQ with 10 mol% SQ-DT and 5 mol% SQ-RGD)) and different UV exposure times (0 min and 3 min) and with/without mechanical loading (strain: 2%, frequency: 1Hz).

(A) s-GAGs content normalized to wet cell-laden hydrogel weight. (B) Quantification of extracted DNA. (C) s-GAGs content normalized to the DNA content. All the cell laden hydrogels were maintained in chondrogenic media containing TGF-β1.

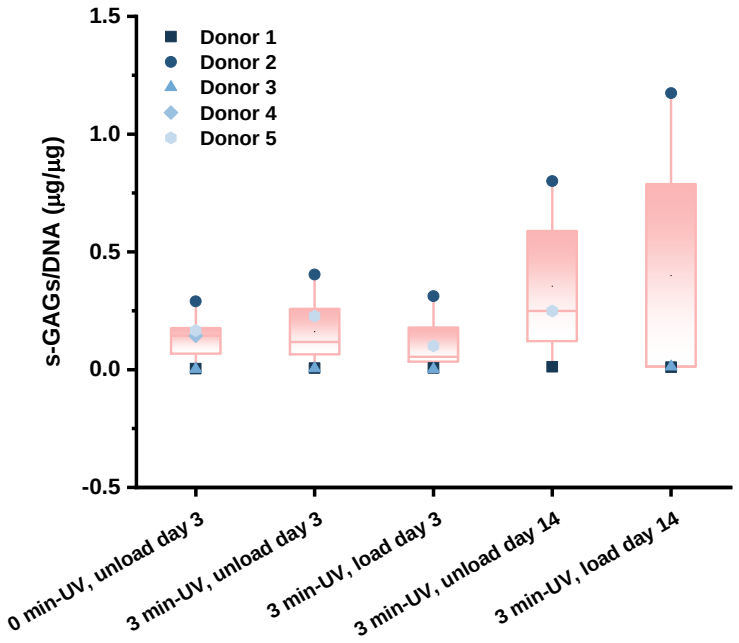

Figure S32. Results of biochemical analysis of s-GAGs content normalized to the DNA content after culture days 3 and 14 of hPACs (donor 1-5) in cell-laden **DN** hydrogels (3.6 wt% **PN** and 5 mM **SN** (SQ with 10 mol% SQ-DT and 5 mol% SQ-RGD)) and different UV exposure times (0 min and 3 min) and with/without mechanical loading (strain: 2%, frequency: 1Hz). All the cell laden hydrogels were maintained in chondrogenic media containing TGF-β1.

Table S4. Normalized s-GAGs per DNA relative to the control (0 min-UV, unload on day 3) of the different donors.

	Donor 1	Donor 2	Donor 3	Donor 4	Donor 5	AVG	SD	*P*-value	*P*-value
				Relative change GAG/DNA					
0 min-UV, unload day 3	1.0	1.0	1.0	1.0	1.0	1.0	0.0		
3 min-UV, unload day 3	1.5	1.4	1.7	/	1.4	1.5	0.1	[a]7.3×10^{-5}	
3 min-UV, load day 3	1.6	1.1	0.8	/	0.6	1.0	0.4	[b]7.7×10^{-2}	
3 min-UV, unload day 14	2.58	2.76	/	/	1.50	2.28	0.6825	/	[d]6.3×10^{-2}
3 min-UV, load day 14	2.28	4.04	3.79	/	/	3.37	0.9547	[c]1.8×10^{-1}	[e]6.3×10^{-3}

[a]: *P*-value of 3 min-UV, unload day 3 *vs.* 0 min-UV, unload day 3.
[b]: *P*-value of 3 min-UV, load day 3 *vs.* 3 min-UV, unload day 3.
[c]: *P*-value of 3 min-UV, load day 14 *vs.* 3 min-UV, unload day 14.
[d]: *P*-value of 3 min-UV, unload day 14 *vs.* 3 min-UV, unload day 3.
[e]: *P*-value of 3 min-UV, load day 14 *vs.* 3 min-UV, load day 3.

Immunocytochemical staining

To visualize collagen type II and fibronectin 1 after culture day 5, the cell-laden hydrogels were first fixed with paraformaldehyde (4%) at RT for 15 min. After washing the hydrogels for 3 times with

PBS, the cells were permeabilized using Triton X-100 solution (0.5%) in PBS at RT for 10 min. The cell-laden hydrogels were washed with PBS (3 x 500 µL) at RT for 5 min. Antigen retrieval was accomplished with Proteinase K treatment (5 µg/mL) at 37°C for 10 min, followed by hyaluronidase treatment (5 mg/mL) at 37°C for 30 min. After washing with PBS (3 x 500µL) for 5 min and blocking of non-specific binding with normal goat serum (NGS, 5%) in PBS at RT for 1 h, the hydrogels were incubated overnight at 4°C with the mixed primary antibodies containing anti-COL II mouse MAB1330 Millipore (1:100) and anti-FN (ab2413, Abcam, 1:100) in the blocking solution (5% NGS in PBS). Then the hydrogels were washed with PBS (3 x 500µL) and incubated at RT for 1 hour with secondary antibodies containing goat anti-mouse Alexa Fluor 647 (1:500) and goat anti-rabbit Alexa Fluor 488 (1:500) in block solution (5% NGS in PBS). After 3 times washing PBS, the hydrogels were covered with VECTASHIELD Antifade Mounting Medium with DAPI at RT for 5 min prior to imaging.

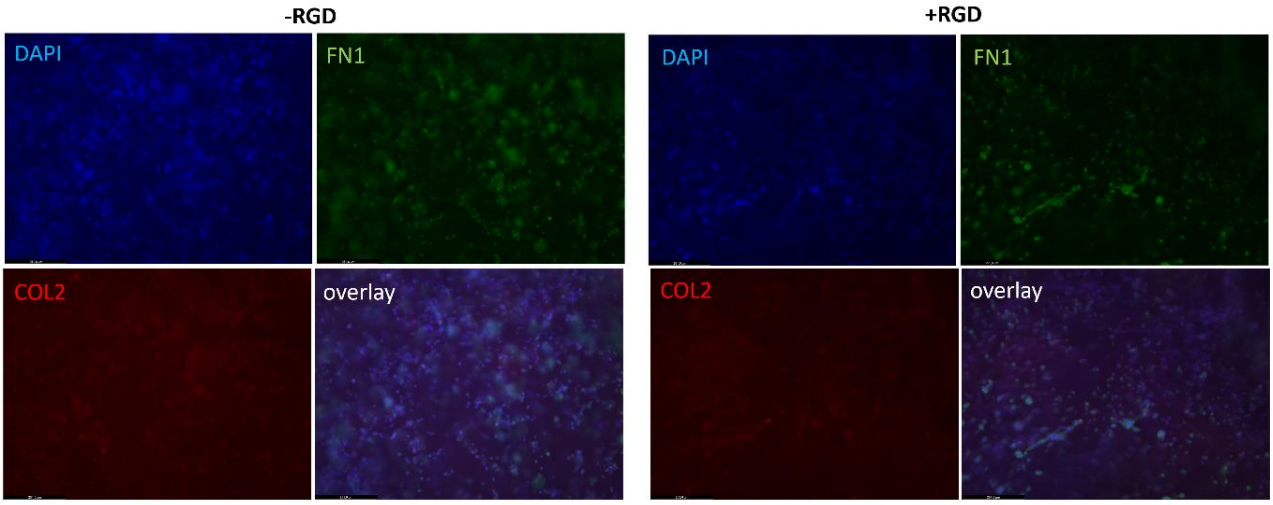

Figure S33. Representative immunofluorescent staining images of hPAC cell-laden **DN** hydrogels (3.6 wt% **PN** and 5 mM **SN** (SQ with 10 mol% SQ-DT) with and without 5 mol% SQ-RGD after 5 days in culture in chondrogenic media containing TGF-β1 with 3 min UV exposure (DAPI for blue, FN1 for green, Type II collagen for red and its overlay). Scale bar: *100 µm*.

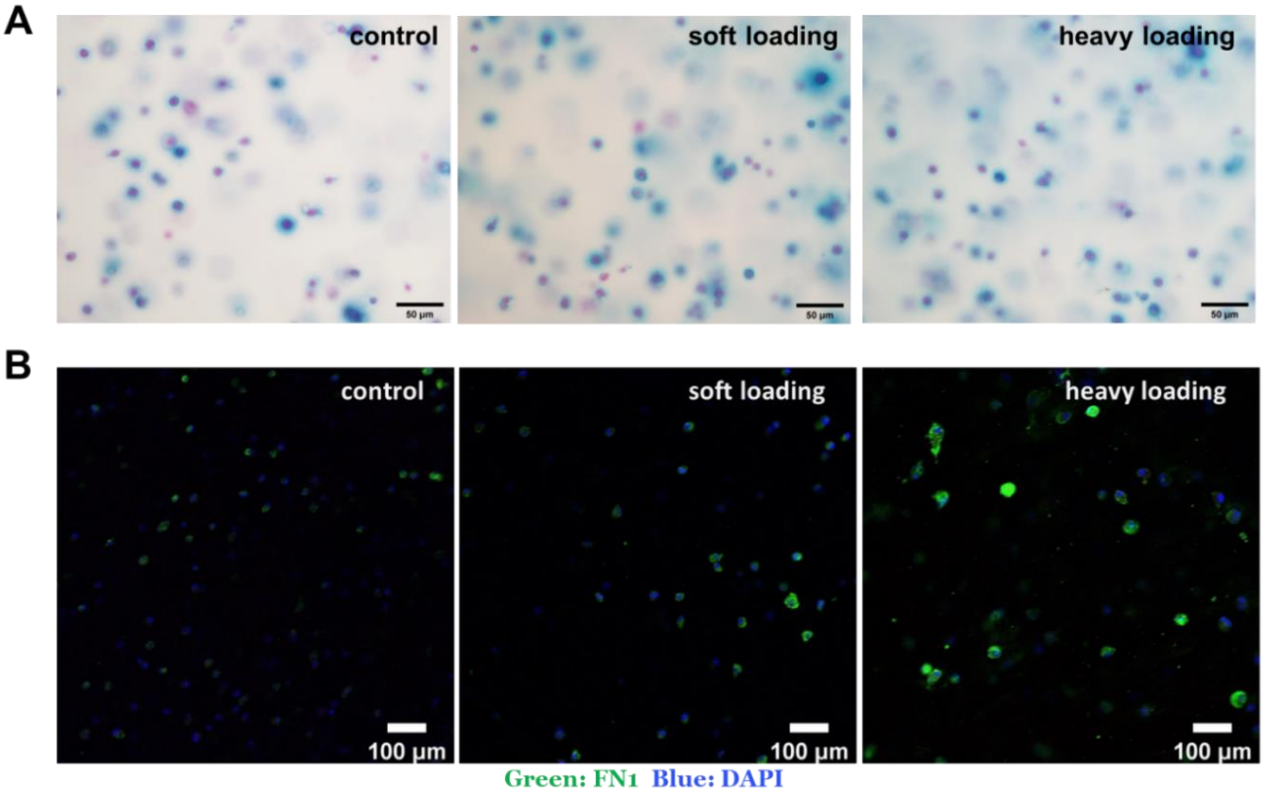

Figure S34. Representative Alcian Blue (A) and immunofluorescent staining (B) images of hPAC cell-laden **DN** hydrogels (3.6 wt% **PN** and 5 mM **SN** (SQ with 10 mol% SQ-DT and 5% molar SQ-RGD)) and with different types of mechanical loading (unloaded control, soft and heavy loading) after culture day 3 in chondrogenic media containing TGF-β1 with 3 min UV exposure (DAPI for blue, FN1 for green, and Type II collagen for red).

Reference

(1) Tong, C.; Wondergem, J. A. J.; Heinrich, D.; Kieltyka, R. E. Photopatternable, Branched Polymer Hydrogels Based on Linear Macromonomers for 3D Cell Culture Applications. *ACS Macro Lett.* **2020,** *9* (6), 882.

(2) Tong, C.; Wondergem, J. A. J.; van den Brink, M.; Kwakernaak, M. C.; Chen, Y.; Hendrix, M.; Voets, I. K.; Danen, E. H. J.; Le Devedec, S.; Heinrich, D.et al. Spatial and Temporal Modulation of Cell Instructive Cues in a Filamentous Supramolecular Biomaterial. *ACS Appl. Mater. Interfaces* **2022,** *14* (15), 17042.

(3) Kim, S. W.; Kim, D. Y.; Roh, H. H.; Kim, H. S.; Lee, J. W.; Lee, K. Y. Three-dimensional bioprinting of cell-laden constructs using polysaccharide-based self-healing hydrogels. *Biomacromolecules* **2019,** *20* (5), 1860.

(4) Yang, F.; Wang, J.; Cao, L.; Chen, R.; Tang, L.; Liu, C. Injectable and redox-responsive hydrogel with adaptive degradation rate for bone regeneration. *J Mater Chem B* **2014,** *2* (3), 295.

(5) Bomer, N.; den Hollander, W.; Ramos, Y. F.; Bos, S. D.; van der Breggen, R.; Lakenberg, N.; Pepers, B. A.; van Eeden, A. E.; Darvishan, A.; Tobi, E. W.et al. Underlying molecular mechanisms of DIO2 susceptibility in symptomatic osteoarthritis. *Ann Rheum Dis* **2015,** *74* (8), 1571.

(6) Farndale, R. W.; Buttle, D. J.; Barrett, A. J. Improved quantitation and discrimination of sulphated glycosaminoglycans by use of dimethylmethylene blue. *Biochimica et Biophysica Acta (BBA)-General Subjects* **1986,** *883* (2), 173.

(7) Liu, J.; Hilderink, J.; Groothuis, T. A.; Otto, C.; Van Blitterswijk, C. A.; de Boer, J. Monitoring nutrient transport in tissue-engineered grafts. *J. Tissue Eng. Regen. Med.* **2015,** *9* (8), 952.

(8) Blonk, J.; Don, A.; Van Aalst, H.; Birmingham, J. Fluorescence photobleaching recovery in the confocal scanning light microscope. *J. Microsc.* **1993,** *169* (3), 363.